

AN EXTENDED HALO-BASED GROUP/CLUSTER FINDER: APPLICATION TO THE DESI LEGACY IMAGING SURVEYS DR8

XIAOHU YANG^{1,2}, HAOJIE XU¹, MIN HE¹, YIZHOU GU¹, ANTONIOS KATSIANIS², JIACHENG MENG³, FENG SHI⁴, HU ZOU⁵, YOUCAI ZHANG⁶, CHENGZE LIU¹, ZHAOYU WANG¹, FUYU DONG⁷, YI LU⁶, QINGYANG LI¹, YANGYAO CHEN^{3,10}, HUIYUAN WANG^{8,9}, HOJUN MO¹⁰, JIAN FU⁶, HONG GUO⁶, ALEXIE LEAUTHAUD¹¹, YU LUO¹², JUN ZHANG¹, YING ZU¹

Draft version April 8, 2022

ABSTRACT

We extend the halo-based group finder developed by Yang et al. (2005b) to use data *simultaneously* with either photometric or spectroscopic redshifts. A mock galaxy redshift survey constructed from a high-resolution N-body simulation is used to evaluate the performance of this extended group finder. For galaxies with magnitude $z \leq 21$ and redshift $0 < z \leq 1.0$ in the DESI legacy imaging surveys (the Legacy Surveys), our group finder successfully identifies more than 60% of the members in about 90% of halos with mass $\gtrsim 10^{12.5} h^{-1} M_{\odot}$. Detected groups with mass $\gtrsim 10^{12.0} h^{-1} M_{\odot}$ have a purity (the fraction of true groups) greater than 90%. The halo mass assigned to each group has an uncertainty of about 0.2 dex at the high mass end $\gtrsim 10^{13.5} h^{-1} M_{\odot}$ and 0.40 dex at the low mass end. Groups with more than 10 members have a redshift accuracy of ~ 0.008 . We apply this group finder to the Legacy Surveys DR8 and find 5.2 Million groups with at least 3 members. About 387,000 of these groups have at least 10 members. The resulting catalog containing 3D coordinates, richness, halo masses, and total group luminosities, is made publicly available.

Subject headings: Dark matter (353); Dark matter distribution (356); Large-scale structure of the universe (902); Galaxies (573); Galaxy groups (597); Galaxy clusters (584); Galaxy dark matter halos (1880)

1. INTRODUCTION

The past two decades have seen great progress in establishing the connection between galaxies and dark matter halos, as parameterized via either the conditional luminosity function (CLF) or the halo occupation distribution (HOD; e.g., Jing et al. 1998; Peacock & Smith 2000; Yang et al. 2003; van den Bosch et al. 2003, 2007; Zheng et al. 2005; Tinker et al. 2005; Mandelbaum et al. 2006; Brown

et al. 2008; More et al. 2009; Cacciato et al. 2009; Neistein et al. 2011; Avila-Reese et al. 2011; Leauthaud et al. 2012). The galaxy-dark matter connection describes how galaxies with different properties occupy halos of different mass and contains important information about how galaxies form and evolve in dark matter halos (see Mo et al. 2010, for a concise review).

Apart from establishing these empirical models, a more direct way of studying the galaxy-halo connection is using galaxy groups, provided that these galaxy groups are defined as sets of galaxies that reside in the same dark matter halos.¹³ Using a well-defined galaxy group catalog, we can not only study the properties of galaxies as a function of their group properties or how the member galaxies evolve within different environments (e.g., Yang et al. 2005a; Collister & Lahav 2005; van den Bosch et al. 2005; Robotham et al. 2006; Zandivarez et al. 2006; Weinmann et al. 2006) but also probe how dark matter halos trace the large-scale structure of the universe (e.g. Yang et al. 2005c, 2006; Coil et al. 2006).

Thanks to many large scale surveys that have been carried out during the past few decades, numerous group catalogs have been constructed, such as the CfA redshift survey (e.g., Geller & Huchra 1983), the Las Campanas Redshift Survey (e.g., Tucker et al. 2000), the 2-degree Field Galaxy Redshift Survey (e.g., Merchán & Zandivarez 2002; Eke et al. 2004; Yang et al. 2005b; Tago et al. 2006; Einasto et al. 2007), the high-redshift DEEP2 survey (Gerke et al. 2005), the Two Micron All Sky Redshift Survey (2MASS; e.g., Crook et al. 2007; Díaz-Giménez & Zandivarez 2015; Lu et al. 2016; Lim et al. 2017),

¹³ In this paper, we refer to a system of galaxies as a group regardless of its richness, including isolated galaxies (i.e., groups with a single member) and rich clusters of galaxies.

¹ Department of Astronomy, School of Physics and Astronomy, and Shanghai Key Laboratory for Particle Physics and Cosmology, Shanghai Jiao Tong University, Shanghai 200240, China; E-mail: xyang@sjtu.edu.cn

² Tsung-Dao Lee Institute, and Key Laboratory for Particle Physics, Astrophysics and Cosmology, Ministry of Education, Shanghai Jiao Tong University, Shanghai 200240, China

³ Department of Astronomy, Tsinghua University, Beijing 100084, China

⁴ Korea Astronomy and Space Science Institute, Yuseong-gu, Daedeok-daero 776, Daejeon 34055, Korea

⁵ Key Laboratory of Optical Astronomy, National Astronomical Observatories, Chinese Academy of Sciences, Beijing 100012, China

⁶ Key Laboratory for Research in Galaxies and Cosmology, Shanghai Astronomical Observatory; Nandan Road 80, Shanghai 200030, China

⁷ School of Physics, Korea Institute for Advanced Study, 85 Heogiro, Dongdaemun-gu, Seoul, 02455, Republic of Korea

⁸ Key Laboratory for Research in Galaxies and Cosmology, Department of Astronomy, University of Science and Technology of China, Hefei, Anhui 230026, China

⁹ School of Astronomy and Space Science, University of Science and Technology of China, Hefei Anhui 230026, China

¹⁰ Department of Astronomy, University of Massachusetts Amherst, MA 01003, USA

¹¹ Department of Astronomy and Astrophysics, University of California, Santa Cruz, 1156 High Street, Santa Cruz, CA 95064, USA

¹² Purple Mountain Observatory, No. 10 Yuanhua Road, Nanjing 210033, China

the zCOSMOS (Wang et al. 2020) and most notably the Sloan Digital Sky Survey (SDSS). Based on SDSS observations, various group catalogs have been constructed with a friends-of-friends (FOF) algorithm (e.g., Goto 2005; Berlind et al. 2006; Merchán & Zandivarez 2005), the C4 algorithm (e.g., Miller et al. 2005), and the halo-based group finder developed in Yang et al. (2005b) (e.g., Weinmann et al. 2006; Yang et al. 2007, 2012; Duarte & Mamon 2015; Rodriguez & Merchán 2020). Among these group finders, the halo-based group finder established in Yang et al. (2005b, 2007) has the particular advantage that it links galaxies to their common dark matter halos (e.g., Campbell et al. 2015). Along this line, efforts were also made to improve the halo mass estimations (e.g., Lu et al. 2015; Wang et al. 2020; Tinker 2020).

Based on the galaxy groups constructed from large redshift surveys, nowadays we can directly measure the halo occupation distribution or the conditional luminosity functions of galaxies in halos of different masses (e.g. Yang et al. 2005a; Yang et al. 2008, 2009; Rodriguez et al. 2015; Lan et al. 2016), study the dependence of galaxy properties on their host halos, e.g. the *galactic conformity* found by Weinmann et al. (2006) (see also Knobel et al. 2015; Kawinwanichakij et al. 2016; Darvish et al. 2017) or the halo and stellar mass quenching factors disentangled by Wang et al. (2018), and measure the group-galaxy cross-correlation function to evaluate how galaxies are distributed within and beyond their host halos (e.g. Yang et al. 2005d; Coil et al. 2006; Knobel et al. 2012). Since galaxy groups trace the dark matter halos we can also stack groups with similar masses, to probe the weak signals of Sunyaev-Zel’dovich (SZ) effects (e.g. Li et al. 2011; Vikram et al. 2017; Lim et al. 2018, 2020) and weak gravitational lensing signals (e.g. Mandelbaum et al. 2006; Yang et al. 2006; Han et al. 2015; Viola et al. 2015; Luo et al. 2018) over a large halo mass range.

In addition to the large spectroscopic redshift surveys, which are usually expensive and observationally time-consuming, photometric redshift surveys in recent years have provided two orders of magnitude more galaxies for our studies. Group/cluster catalogs have also been constructed from these photometric redshift data, especially from SDSS observations. For example, Goto et al. (2002) developed a cut-and-enhance method and applied it to the early SDSS commissioning data. Bahcall et al. (2003) used two different selection methods including a hybrid matched filter method (Kim et al. 2002) and a “maxBCG” method to find clusters. Lee et al. (2004) identified compact groups in the SDSS Early Data Release. Koester et al. (2007) identified clusters using the maxBCG red-sequence method from the SDSS DR5. citetLiu2008 developed a probability FOF method and tested it using DEEP2 mock catalogs. Hao et al. (2010) used a GMBCG method to find clusters in SDSS DR7. Szabo et al. (2011) constructed a cluster catalog from SDSS DR6 using an adaptive matched filter cluster finder. Wen et al. (2012) created a cluster catalog using the photometric redshifts of galaxies from SDSS III. Rykoff et al. (2014) constructed a cluster catalog using the red-sequence cluster finder, redMaPPer, from SDSS DR8. Oguri et al. (2018) constructed a cluster catalog from the Hyper Suprime-Cam (HSC) Subaru Strategic Program using the CAMIRA algorithm.

The above group/cluster-finding algorithms applied to

the photometric redshift data are mainly based on either the red-sequence feature or the overdensity feature of the clusters, which require either the existence of the brightest cluster galaxy or an overdensity peak as the candidate cluster location. Thus, the group/cluster catalogs constructed may suffer from incompleteness due to the lack of BCG observation, or the threshold of the overdensity, or contamination caused by the foreground and background galaxies. In general, only the rich clusters of these catalogs are reliable tracers of the overall cluster population. In this work, to make better use of the available photometric redshift survey data, we propose to extend the halo-based group finder developed in Yang et al. (2005b, 2007) (hereafter, Y05 and Y07), so that it can be applied to both photometric and spectroscopic redshift surveys. We will see that this extended group/cluster finder has better performance for the group completeness which is important for cosmological studies and better performance for the group membership determination which is important for galaxy formation studies. After testing our extended group finder on the mock photometric redshift galaxy survey, we employed it to the currently largest photometric redshift galaxy sample, the DESI legacy image surveys (hereafter the Legacy Surveys) DR8 galaxy catalog, and generated group/cluster catalogs for subsequent investigations.

This paper is organized as follows: In Section 2 we provide a detailed description of the data we use for our investigation, including the Legacy Surveys DR8 galaxy catalog and the mock redshift surveys. In Section 3 we describe the main steps adopted for our extended halo-based group finder. The performance of this group finder is tested in Section 4. In Section 5 we present some of the basic properties of the groups we extract from the Legacy Surveys DR8. Finally, we summarize our results in Section 6. For the observational data, we adopt a Λ CDM cosmology with parameters that are consistent with the Planck 2018 results (Planck Collaboration et al. 2020, hereafter Planck18 cosmology): $\Omega_m = 0.315$, $\Omega_\Lambda = 0.685$, $n_s = 0.965$, $h = H_0/(100 \text{ km s}^{-1} \text{ Mpc}^{-1}) = 0.674$ and $\sigma_8 = 0.811$.

2. THE DATASET

In this section, we describe the data used in this study: (i) the galaxy catalog with photometric redshifts obtained from the Legacy Surveys and the spectroscopic redshifts from various sources, (ii) the mock galaxy catalogs generated from N-body simulations to test the performance of our group/cluster finder.

2.1. DESI Legacy Imaging Surveys DR8

The DESI Legacy Imaging Surveys provide the target catalogs for the DESI survey. The target selection requires a combination of three optical (*grz*) bands and two mid-infrared (W1 $3.4\mu\text{m}$, W2 $4.6\mu\text{m}$) bands. For the case of galaxies, the *g/r/z* bands have at least a 5σ detection of $24/23.4/22.5$ AB magnitude with an exponential light profile of half-light radius $0''.45$. The optical imaging data are provided by three public projects: the *Beijing-Arizona Sky Survey* (BASS), the *Mayall z-band Legacy Survey* (MzLS), and the *DECam Legacy Survey* (DECaLS), while the *Wide-field Infrared Survey Explorer* (WISE) satellite provides the infrared data. See

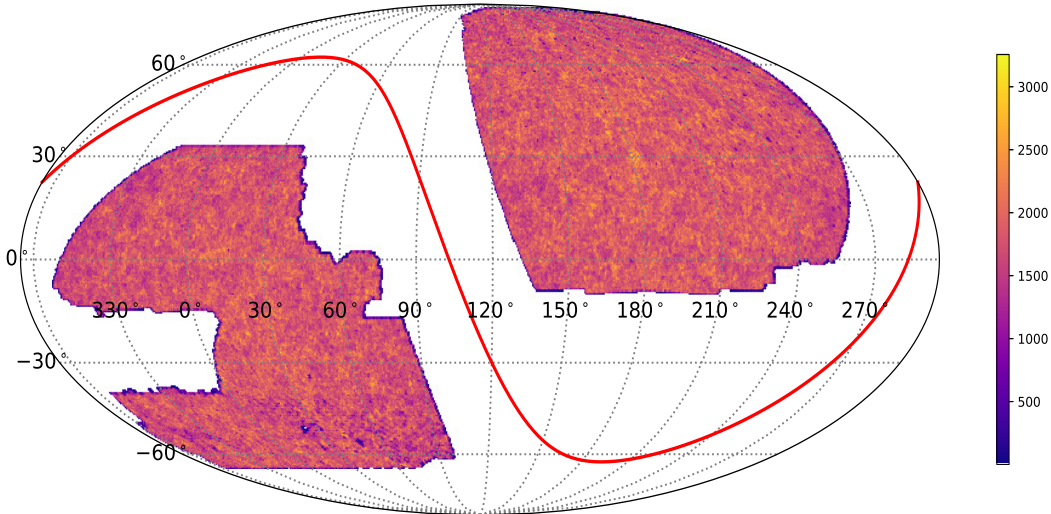


FIG. 1.— The sky coverage of galaxies. These are drawn from two contiguous areas: the south galactic cap (~ 8580 square degrees with 59.6 million galaxies) and the north galactic cap (~ 9673 square degrees with 69.75 million galaxies). The color code is the galaxy number counts per 0.25 square degrees.

an overview of the surveys in Dey et al. (2019).

We select our sample from the latest public data release of the Legacy Surveys, the Data Release 8 (DR8). DR8 also includes data from some non-DECaLS surveys, with the majority originating from the *Dark Energy Survey* (DES). The catalogs are processed by the software package THE TRACTOR (Lang et al. 2016) for source detection and optical photometry.

Our galaxy samples first select those object with morphological classification as type *REX*, *EXP*, *DEV* and *COMP* from Tractor fitting results¹⁴.

Following suggestions from the DESI Target selection (also see Zou et al. 2019; Zhou et al. 2020a; Ruiz-Macias et al. 2020; Zhou et al. 2020b; Raichoor et al. 2020; Yèche et al. 2020), we require objects to have at least one exposure in each optical band and remove the area within $|b| < 25.0^\circ$ (where b is the Galactic latitude) to avoid high stellar density regions. In addition to the Tractor morphology selection, a minimum data quality flags are employed to remove the flux contaminations from nearby sources (FRACFLUX) or masked pixels (FRACMASKED):

$$\begin{aligned} \text{FRACMASKED}_i &< 0.4 \\ \text{FRACIN}_i &> 0.3 \\ \text{FRACFLUX}_i &< 0.5 \end{aligned}$$

where $i \equiv g, r, z$. FRACIN is to select the objects for which a large fraction of the model flux is in the contiguous pixels where the model was fitted. We also remove any objects close to bright stars by masking out objects with the following bits number in DR8 *MASKBITS* column: 1 (close to Tycho-2 and GAIA bright stars), 8 (close to WISE W1 bright stars), 9 (close to WISE W2 bright stars), 11 (close to fainter GAIA stars), 12, and 13 (close to an LSIGA large galaxy and globular cluster,

¹⁴ In the Tractor fitting procedure, *REX* stands for round exponential galaxies with a variable radius, *DEV* for deVaucouleurs profiles (elliptical galaxies), *EXP* for exponential profiles (spiral galaxies), and *COMP* for composite profiles that are deVaucouleurs plus exponential (with the same source center).

respectively). Note that all the magnitudes used in this paper are in the AB system and have been corrected for Galactic extinction by using the Galactic transmission values provided in DR8.

We adopt the random forest algorithm based photometric redshift estimation for the galaxies in our sample from the *Photometric Redshifts for the Legacy Surveys* (*PRLS*¹⁵, Zhou et al. 2020a). To ensure the photo- z quality in the sample, we further limit our analysis to galaxies with $z \leq 21$ (above which the photometric redshifts are not reliable) and $0 < z_{\text{phot_median}} \leq 1$, where the $z_{\text{phot_median}}$ is the median value of photo- z probability distribution function (PDF). See the details regarding the photometric redshift training and performance in appendix B of Zhou et al. (2020a). To make the sample's redshift information as accurate as possible, we replace the photometric redshift with the spectroscopic redshift, if available. In total, there are 2.1 million galaxies with spectroscopic redshifts in our sample. The complete spectroscopic redshifts sources in the original catalog include: BOSS, SDSS, WiggleZ, GAMA, COSMOS2015, VIPERS, eBOSS, DEEP2, AGES, 2dFLenS, VVDS, and OzDES¹⁶. Additional spectroscopic redshifts were obtained by matching galaxies in our sample with those in 2MASS Redshift Survey (2MRS; Huchra et al. 2012), 6dF Galaxy Survey Data Release 3 (6dFGRS; Jones et al. 2009), and 2dF Galaxy Redshift Survey (2dFGRS; Colless et al. 2001).

After applying all the above selection criteria, we have a total number of 129.35 million galaxies remaining in our sample, within which 69.75 million are located in the north galactic cap (NGC) and 59.6 million in the south galactic cap (SGC). The total sky coverage of the galaxy sample is 18,253 square degrees (9673 square degrees in NGC, 8580 square degrees in SGC). As an illustration, we show the final footprint of galaxies on the sky in Figure 1.

For each galaxy in our NGC and SGC samples, ac-

¹⁵ <https://www.legacysurvey.org/dr8/files/#photometric-redshift-files-8-0-photo-z-sweep-brickmin-brickmax-pz-fits>

¹⁶ Check the selection conditions in these surveys in section 3.2, Zhou et al. 2020a.

cording to the typical photoz errors in the Legacy Surveys DR8 photoz galaxy catalog (e.g. Zhou et al. 2020a; Wang et al. 2020), we assign it with a photometric redshift error,

$$\sigma_{\text{photo}} = 0.01 + 0.015z. \quad (1)$$

If a galaxy has a spectroscopic redshift, we set $\sigma_{\text{photo}} = 0.0001$. This value will be used in our modified group finder.

Next, for each galaxy, we use the following function to convert apparent magnitude to absolute magnitude according to its redshift,

$$M_z - 5 \log h = m_z - \text{DM}(z) - K_z^{0.5}$$

where $\text{DM}(z)$ is the distance module corresponding to redshift z ,

$$\text{DM}(z) = 5 \log D_L(z) + 25$$

with $D_L(z)$ being the luminosity distance in $h^{-1}\text{Mpc}$. $K_z^{0.5}$ represents the K-correction in z-band to sample median redshift $z \sim 0.5$, obtained from the ‘Kcorrect’ model (eg. v4.3) described in Blanton & Roweis (2007). For illustration, Fig. 2 shows $K_z^{0.5}$ values for a subset of our sample galaxies.

In general, the average K-correction can be described by the following function,

$$K_z^{0.5}(z) = az^2 + bz + c. \quad (2)$$

The fits to the median $K_z^{0.5}$ values in the redshift bin of 0.01 result is shown in Fig.2 as the red line with $\{0.86 \pm 0.06, -0.67 \pm 0.06, -0.3 \pm 0.01\}$ for $\{a, b, c\}$, respectively. For the mean $K_z^{0.5}$ values in the redshift bin of 0.01, the fitting result is $\{0.73 \pm 0.05, -0.54 \pm 0.05, -0.33 \pm 0.01\}$ for $\{a, b, c\}$. The fits agrees quite well with the overall K-correction trend. We will use the best fitting results to the median $K_z^{0.5}$ values to model the K-correction of galaxies in our mock redshift surveys, as well as in calculating the maximum redshift a galaxy can be observed in the next subsection.

The luminosity of each galaxy is then calculated using the following formula:

$$\log_{10} L = 0.4 * (4.80 - M_z)$$

with taking K-correction of the sun, $K_z^{0.5}(0.0) = -0.3$, into account, to be consistent with M_{\odot} being 4.5 in z-band (Willmer 2018).

2.2. Simulation and mock galaxy redshift survey

The N-body simulation used in our study is the ELUCID simulation carried out at the High Performance Center (HPC) at the Shanghai Jiao Tong University (Wang et al. 2016). ELUCID evolves the distribution of 3072^3 dark matter particles in a periodic box of $500 h^{-1}\text{Mpc}$ (L_{500}) from redshift $z = 100$ to $z = 0$. The simulation was run with the code L-GADGET, a memory-optimized version of GADGET2 (Springel 2005). The cosmological parameters adopted by ELUCID are consistent with the WMAP5 results and are the following: $\Omega_m = 0.258$, $\Omega_b = 0.044$, $\Omega_{\Lambda} = 0.742$, $h = 0.72$, $n_s = 0.963$ and $\sigma_8 = 0.796$ while each particle has a mass of $3.0875 \times 10^8 h^{-1}M_{\odot}$. The simulation is constrained (in terms of initial conditions) by the re-constructed initial density field of SDSS DR 7 (Wang et al. 2014). ELUCID

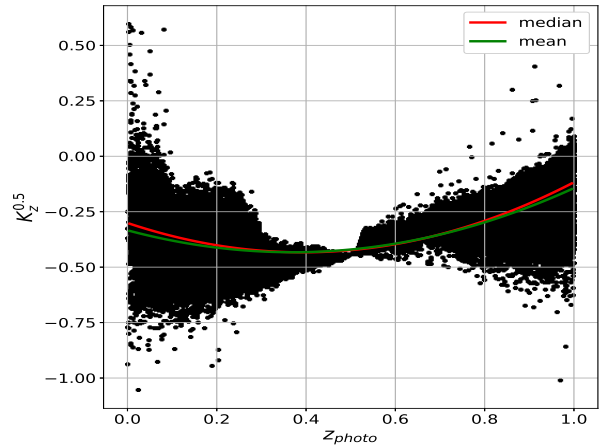


FIG. 2.— K-correction to sample median redshift 0.5. We show a random subset (50,000) of the sample galaxies, with the red (green) line fitting to the median (mean) K-correction in redshift bins of 0.01.

has been already used to study galaxy quenching (Wang et al. 2018), galaxy intrinsic alignment (Wei et al. 2018), and cosmic variance (Chen et al. 2019) while it was also combined with the abundance matching method to evaluate galaxy formation models (Yang et al. 2018) and the L-Galaxies semi-analytic model (Katsianis et al. 2020).

Dark matter halos were identified with the standard Friend-of-Friends (FoF) algorithm (Davis et al. 1985) with a link length equal to 0.2 times the average particle separation and with at least 20 particles. The halo mass is calculated by summing up the mass of all the particles linked to the dark matter halo. As shown in Wang et al. (2016), the halo mass function obtained from this simulation is in good agreement with the analytic model prediction by Sheth et al. (2001) (SMT2001) at the mass ranges of interest. Based on halos at different outputs, halo merger trees were constructed (see Lacey & Cole 1993). A halo in an earlier output is considered to be a progenitor of a present halo if more than half of its particles are found in the present halo. The main branch of a merger tree is defined as all the progenitors going through from the bottom to the top, choosing always the most massive branch at every branching point. These progenitors are labeled as the main-branch progenitors. Based on the above merger trees, galaxy catalogs were generated using the empirical galaxy formation model described in Chen et al. (2019). Note that by combing the true and Monte Carlo merger trees, we have generated galaxies in all the halos in our ELUCID simulations with mass $\geq 10^9 h^{-1}M_{\odot}$, with a minimum galaxy luminosity below $10^8 h^{-2}L_{\odot}$ in all the simulation snapshots that we are going to use.

In this study, we create a mock galaxy redshift survey (MGRS) from the above-constructed galaxy catalogs. The MGRS, with z-band galaxy magnitude $z \leq 21$, spans a redshift range of $0.0 < z \leq 1.1$, maximum angles of $\Delta\delta = 10.0^\circ$, $\Delta\alpha = 20.0^\circ$ and thus a total sky coverage at 199.74 deg^2 . Here we have taken into a negative K-correction to obtain the apparent magnitude for each galaxy. Since the redshift range we are interested in, $0.0 < z < 1.1$, is quite large, we have taken into account the light cone effect by stacking simulation boxes at different redshifts that are most consistent with the

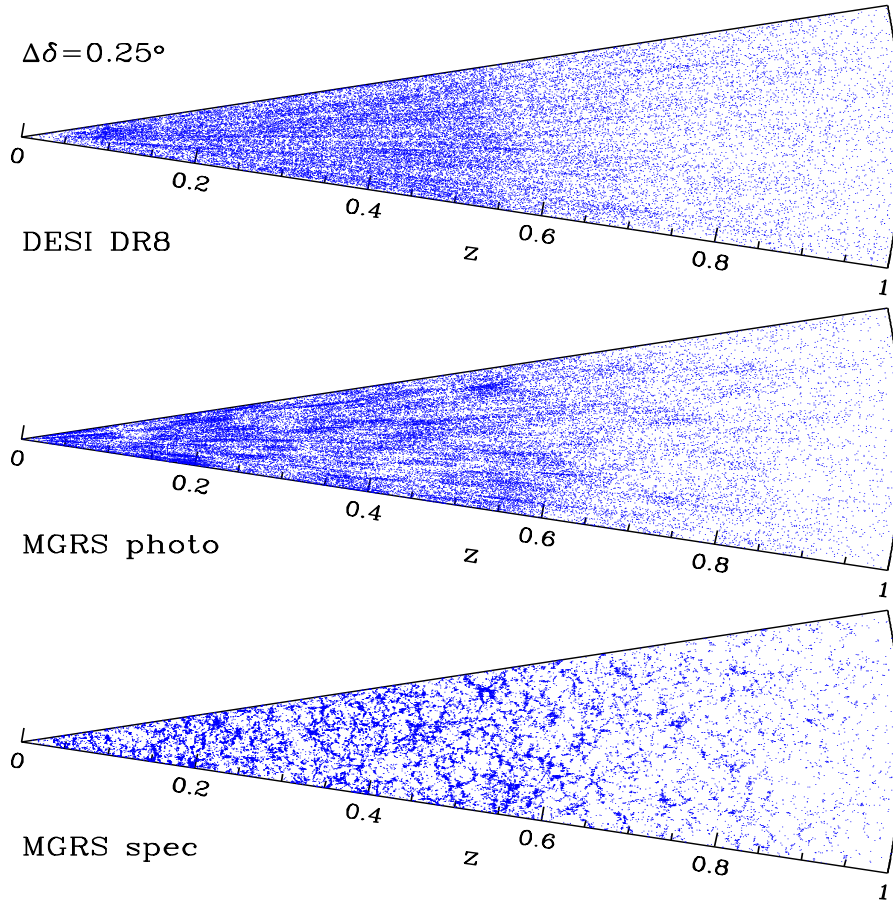


FIG. 3.— Lower panel: the projected distribution of a small subset of galaxies along the declination direction (with $\Delta\delta = 0.25^\circ$) in the mock spectroscopic redshift survey. Middle panel: same as the lower panel, but for the mock photometric redshift survey, where galaxies are added with additional photometric redshift errors specified by Eq. 1. Upper panel: the projected distribution of a subset of galaxies in the Legacy Surveys DR8.

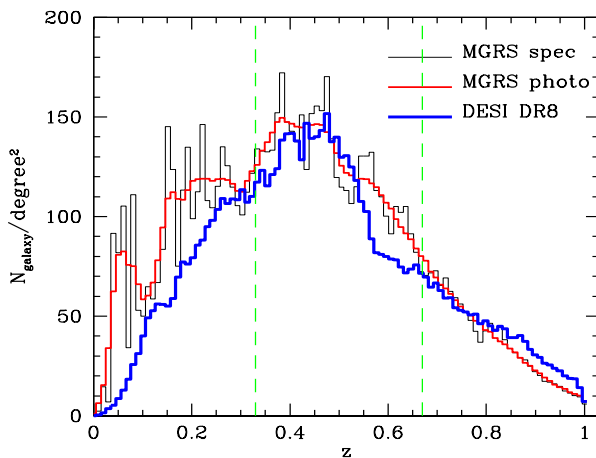


FIG. 4.— The redshift distribution of galaxies in our MGRS and DESI DR8 samples, where the number of galaxies is normalized with respect to the sky coverage of the sample. The galaxy samples are separated into three redshift bins as indicated by the vertical dashed lines.

redshifts where they locate. The details of making the MGRS is described in Meng et al. (2020).

On top of the redshift information from the mock galaxy catalog, we assign each galaxy a random shift drawn from a Gaussian distribution with dispersion

$\sigma_{\text{photo}}*(1+z)$, where σ_{photo} is the typical photoz errors in the Legacy Surveys DR8 photoz galaxy catalog described by Eq.1. This value is also kept in the MGRS for our modified group finder to use. We select galaxies with redshifts $0.0 < z \leq 1.0$ from the mock galaxy catalog. There are a total of 1681566 and 1679924 galaxies remaining in our mock spectroscopic and photometric redshift surveys, respectively. As an illustration, we show the projected distribution of a small subset of galaxies along the declination direction (with $\Delta\delta = 0.25^\circ$) within redshift $0.0 < z \leq 1.0$ in Fig. 3, where the lower and middle panels show our results for the mock spectroscopic and photometric redshift surveys, respectively. Compared to the clear cosmic web structures shown for the spectroscopic MGRS, galaxies in the photometric MGRS have more stretched structures along the line-of-sight. For comparison, we present the distribution of a small subset of galaxies in the Legacy Surveys DR8 in the upper panel of Fig. 3. The overall features in the photometric MGRS and the Legacy Surveys DR8 are quite similar.

Once the MGRS is generated, we provide some intrinsic properties of the groups/clusters. Taking into account the fact that the halo mass functions and group/cluster luminosity functions may change significantly in the redshift range we are probing, we separate galaxies/groups/clusters in our MGRS (as well as our observed galaxy samples) into three redshift bins:

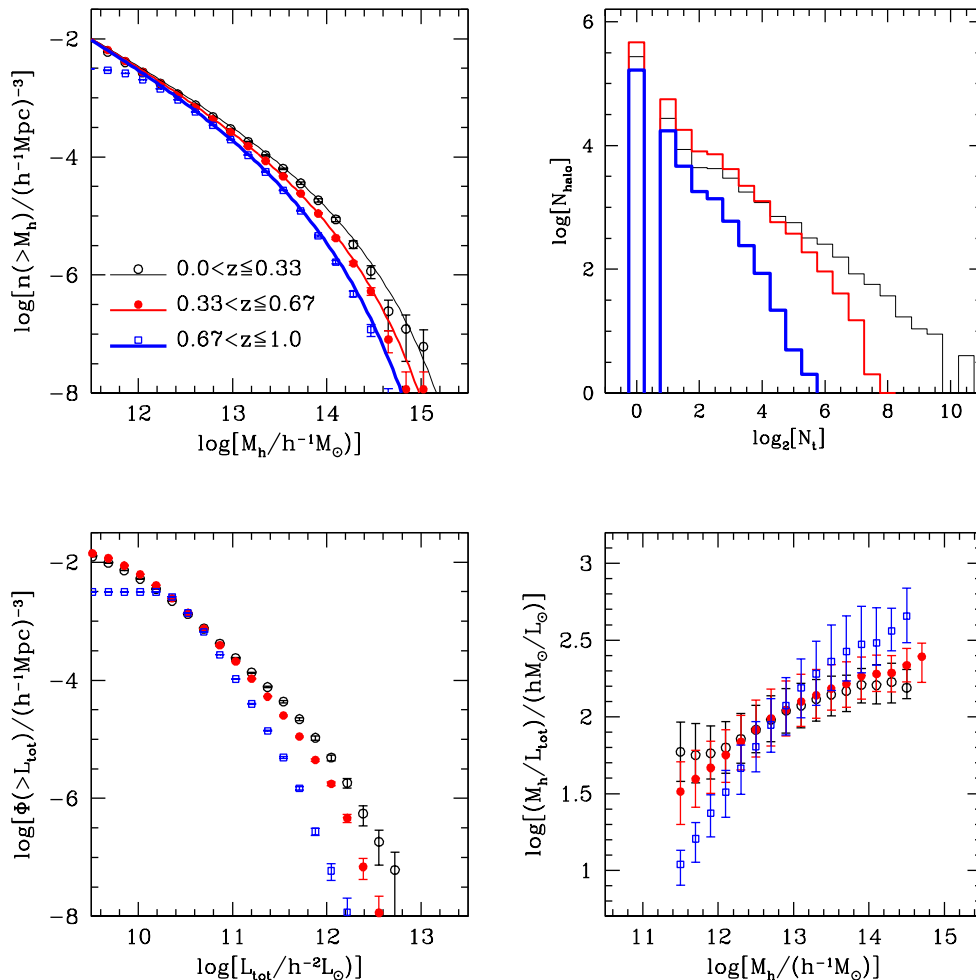


FIG. 5.— Upper left panel: the *accumulative* halo mass functions of groups in different redshift bins as indicated (same color coded for all panels in this figure). The symbols with errorbars are the results measured from the MGRS. The solid lines represent the corresponding theoretical model predictions given by SMT2001 for a WMAP5 cosmology, which match by construction. Upper right panel: the richness distribution of groups in the MGRS. Lower left panel: the *accumulative* group luminosity function, where group luminosity is the sum of luminosity of all member galaxies with apparent magnitude $z \leq 21$ in the same halo. Lower right panel: the median mass-to-light ratio of groups as a function of halo mass in the MGRS. All errors obtained in this plot are estimated using 200 bootstrap resamples.

$0.0 < z \leq 0.33$, $0.33 < z \leq 0.67$, $0.67 < z \leq 1.0$. As an illustration, we show in Fig. 4 the redshift distribution of galaxies in our MGRS and DESI DR8 samples, where the number of galaxies is normalized with respect to the sky coverage of the sample. The vertical dashed lines separate galaxies in our samples into the three redshift bins.

Shown in the upper left panel of Fig.5 are the *accumulative* halo mass functions of groups/clusters in different redshift bins as indicated. Symbols with errorbars are derived from the MGRS. Note that in order to partially reduce the impact of magnitude cut $z \leq 21$, we separate the galaxy samples into $N_{zbin} = 3$ redshift bins and use a V_{max} method to calculate the halo mass functions,

$$n(> M_h) = \sum_i 1/V_{max}, \quad (3)$$

where, i is the ID of the halo/group, V_{max} is calculated according to the apparent magnitude of the brightest group galaxy (BGG) at which redshift, z_{max} , it can be observed,

$$V_{max} = V(\min[z_{max}, z_{bin,up}]) - V(z_{bin,low}). \quad (4)$$

Here $z_{bin,low}$ and $z_{bin,up}$ are the lower and upper limits of the corresponding redshift bin, respectively. In calculating the z_{max} of a galaxy, we have properly taken into account the difference in the K-correction between the actual and maximum redshifts, z_{max} , using Eq. 2. As a comparison, we also show the corresponding theoretical model predictions given by SMT2001 represented by the solid lines. We demonstrate that overall the model and data agree quite well, though some small deviation shown at the high mass end for the low redshift bin, which is mostly caused by the small volume of our sample. On the other hand, the deviation at the low mass end for the high redshift bin, although we have partly corrected using the V_{max} method, is due to the survey magnitude limit cut, $z \leq 21$, where faint galaxies residing in low mass halos can not be observed. In the upper right panel, we present the richness distribution of groups/clusters in the MGRS. In the lowest redshift bin, there are only a few groups with more than 1000 members, while in the high redshift bin, the richest groups host around 30 members. At the lower left panel, we show the *accumulative* total luminosity function of groups/clusters, with the total lu-

minosities L_{tot} calculated by summing up all the member galaxy luminosities with apparent magnitude $z \leq 21$ in the MGRS. Here again, a V_{max} method similar to Eq. 3 is used to partly correct the group incompleteness. Obviously, at the high redshift bin, the groups/clusters with $L_{\text{tot}} < 10^{10.2} h^{-2} L_{\odot}$ are missing from our MGRS, which simply reflects the facts that galaxies in this redshift bin below this luminosity did not meet the magnitude limit cut. In the lower right panel, we present the median mass-to-light ratio of groups/clusters in the MGRS. Overall, the mass-to-light ratio in high mass groups/clusters $\sim 10^{14.5} h^{-1} M_{\odot}$ spans from about 200 at low redshift to about 500 at high redshift. In low mass groups with mass $\sim 10^{11.5} h^{-1} M_{\odot}$ the related numbers decrease to 50 to 10, respectively. Note that all the errorbars obtained in this figure are estimated using 200 bootstrap re-samplings.

2.3. The z -band galaxy luminosity functions

Before we evaluate the group/cluster finding algorithm with the mock catalogs and apply the method to the Legacy Surveys DR8 observational data, we measure the galaxy luminosity functions (LFs) from the mock and observational galaxy catalogs. The galaxy luminosity function, which describes the average light densities of the Universe, represents a fundamental tool in understanding galaxy formation and evolution. Since galaxies are formed within dark matter halos and the most massive (central) galaxies reside roughly in the most massive halos, there exists statistical relations between galaxy luminosities and halo mass (e.g. Yang et al. 2012, and references therein). The accurate estimation of the galaxy luminosity functions plays a key role in establishing those kinds of relations. We estimate the galaxy luminosity function by counting galaxies in each luminosity bin and weighted by $1/V_{\text{max}}$,

$$\Phi(L) d \log L = \sum_i 1/V_{\text{max}}.$$

Here V_{max} can be similarly calculated using Eq. 4, but for the galaxy's own z_{max} .

We first focus on galaxies with mock spectroscopic redshifts in the MGRS. Shown in the left panel of Fig. 6 are the z -band luminosity functions of galaxies in three redshift bins: $0.0 < z \leq 0.33$, $0.33 < z \leq 0.67$, $0.67 < z \leq 1.0$, respectively. The galaxy luminosities are obtained from the z -band absolute magnitude K -corrected to redshift $z = 0.5$. In general, we see that the LFs measured in different redshift bins are roughly consistent with each other at the bright end. Since the MGRS is only complete up to $z \leq 21$, faint galaxies will not be observed, especially those at higher redshifts. Thus, we see that the derived LFs have suffered more from incompleteness problem in the higher redshift bins, with brighter faint luminosity end cutoffs. Again, the errorbars are obtained from 200 bootstrap re-samplings of galaxies.

Next, we focus on galaxies with photometric redshifts in the MGRS. The solid lines shown in the left panel of Fig. 6 are obtained using the mock photometric redshift galaxies. Overall, the results are in good agreement with those obtained from the mock spectroscopic redshift galaxy samples. Since in our mock photometric redshifts,

we only add a small redshift error to each galaxy, without any catastrophic redshift assignment. That is the main reason that we do not see a significant Eddington bias which might be induced in most of the photometric redshift surveys.

Finally, we focus on the Legacy Surveys DR8 data. The symbols shown in the right panel of Fig. 6 are the retrieved galaxy luminosity functions in three redshift bins. Compared to the MGRS (shown as solid lines), galaxies in the Legacy Surveys DR8 show similar cutoffs at low luminosity ends, which is caused by the same $z \leq 21$ magnitude cut. On the other hand, galaxies in the Legacy Surveys DR8 are somewhat brighter. This is mostly due to the galaxy luminosity calibration as well as the different K -correction modelings. Here we used the photometric data in COSMOS2015 catalog (Laigle et al. 2016) to calibrate the luminosity of the galaxies in our catalog. The galaxy luminosity is firstly assigned in y band using a luminosity-stellar mass abundance matching method. Then a z band galaxy luminosity is obtained according to the $z - y$ color of the galaxy, which is obtained using the age distribution matching method (Hearin & Watson 2013). For each galaxy in our catalog, we choose a galaxy with the same luminosity and color in COSMOS2015 and use this galaxy's fitted spectrum to calculate the K -correction and hence the apparent magnitude of that galaxy. See Meng et al. (2020) for more details. Note that since the K -correction used in Meng et al. (2020) was corrected to redshift $z = 0.0$, in order to be consistent with the one used in this paper, we use z -band apparent magnitude and Eq. 2 to calculate the absolute magnitude and luminosity of each galaxy in our MGRS. Nevertheless, since in our cluster finder, we are using the accumulate luminosity functions measured from the data in different redshift bins to estimate the halo mass, such systematic differences will not impact the group/cluster membership determination.

3. THE EXTENDED HALO-BASED GROUP FINDER

The halo-based group finder developed in Yang et al. (2005b, 2007) has been tested and successfully applied to galaxy samples with spectroscopic redshifts (see references listed in the introduction). The strength of the algorithm lies in its iteration nature and utilization of an adaptive filter while taking into account the general properties of dark matter halos. However, it can only be applied to galaxy samples with spectroscopic redshift. In this work, we extend the algorithm so that it can deal with galaxies with photometric and spectroscopic redshift simultaneously.

Below we list the main steps that are used in our extended group finder. Note that the basic framework of this extended halo-based group finder is quite similar to the one used in Y05 and Y07, except those minor changes, the most important extension/upgrade in our extended group finder is related with Eq. 7 in Step 4.

Step 0: Start. We start our search by assuming that each galaxy is a group candidate.

Step 1: Measure the accumulative group luminosity functions. We first measure the total luminosity within each group,

$$L_G = \sum_i L_i, \quad (5)$$

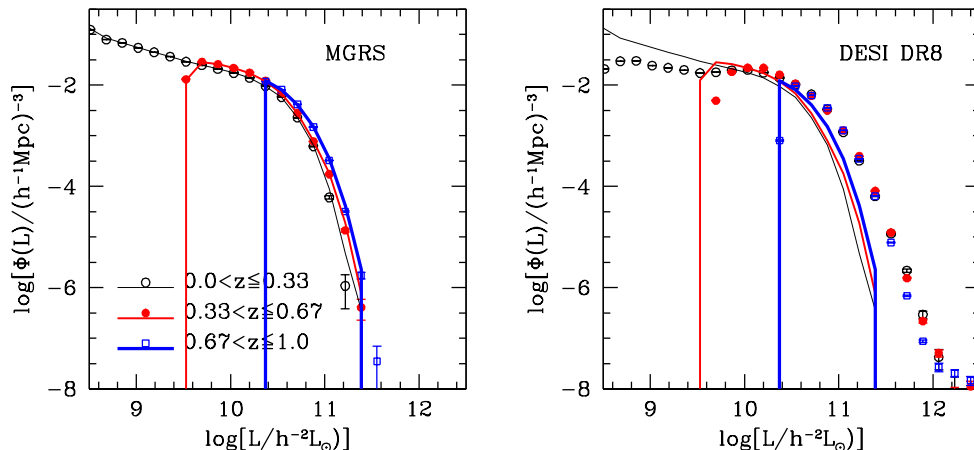


FIG. 6.— Left panel: the galaxy luminosity functions obtained from galaxies in the MGRS. The data points with errorbars are the results obtained from galaxies with mock spectroscopic redshifts in different redshift bins as indicated. The solid lines represent results obtained from galaxies using the mock photometric redshifts correspondingly. Right panel: the galaxy luminosity functions obtained from galaxies in the Legacy Surveys DR8. The Symbols are for galaxies in different redshift bins as those in the left panel. The solid lines are the same as those shown in the left panel for comparison.

where i is the ID and L_i is the luminosity of each member galaxy. Then we calculate the accumulative group luminosity functions from the whole group sample similar to Eq. 3. Note that since the galaxy/group samples from observations are usually flux limited, measurements at different redshifts suffer from different absolute magnitude limits. In order to partially reduce the impact of this observational selection effect, here again we separate the galaxy samples into $N_{z\text{bin}} = 3$ redshift bins and use a V_{max} method to calculate the accumulative group luminosity functions (e.g. Eq. 4).

Step 2: Determine the mass-to-light ratio of the groups. In each redshift bin, the accumulative halo mass function is calculated at the median redshift of the galaxies of interest. The mass-to-light ratios of the groups in each redshift bin are then computed using the abundance matching method according to the accumulative halo mass functions and group luminosity functions (see section 3.5 of Y07). Here we have properly taken into account the incompleteness of the halos/groups as described in Section 4.2.

Step 3: Estimate the mass, size, and velocity dispersion of the dark matter halo associated with each tentative group. With the mass-to-light ratios in different redshift bins determined in step 2, we assign each tentative group with a halo mass, M_L , by interpolations on both the redshift and total luminosity of the group.

In our study, we define dark matter halos as having an overdensity of 180 times the background density of the universe. This corresponds to a comoving halo radius of

$$r_{180} = 0.781 h^{-1} \text{Mpc} \left(\frac{M_L}{\Omega_m 10^{14} h^{-1} M_\odot} \right)^{1/3}$$

where z_{group} is the redshift of the group center. The line-of-sight velocity dispersion of dark matter particles is described by

$$\sigma_{180} = 632 \text{ km s}^{-1} \left(\frac{M_L \Omega_m}{10^{14} h^{-1} M_\odot} \right)^{0.3224}. \quad (6)$$

This fitting function is obtained by van den Bosch et al.

(2004) to describe the halo mass dependence of the one-dimensional velocity dispersion of dark matter particles using the halo concentrations of Macciò et al. (2007). Here slight modifications are made with respect to the ones using in Y07 so that they are applicable to Λ CDM cosmology with other Ω_m values. The best fitting values used in Eq. 6 are obtained from a few sets of simulations with different Ω_m values (Frank C. van den Bosch, private communications).

Step 4: Determine the group memberships using halo information. We sort and start from the most massive group candidate to search its member galaxies using its halo properties. We assume that the distribution of galaxies in phase-space follows that of the dark matter particles and the number density contrast of galaxies in the redshift space around the group center (the luminosity weighted center) at redshift z_{group} can be written as

$$P_M(R, \Delta z) = \frac{H_0 \Sigma(R)}{c \bar{\rho}} p(\Delta z),$$

where c is the speed of light, $\Delta z = z - z_{\text{group}}$, $\bar{\rho}$ is the average density of Universe, and $\Sigma(R)$ is the projected surface density of a (spherical) NFW (Navarro et al. 1997) halo:

$$\Sigma(R) = 2 r_s \bar{\delta} \bar{\rho} f(R/r_s).$$

Readers who are interested in the detailed functional forms within this equation can go to Y07 for more details.

The function $p(\Delta z)d\Delta z$ describes the redshift distribution of galaxies within the halo, and is assumed to have a Gaussian form,

$$p(\Delta z) = \frac{1}{\sqrt{2\pi}} \frac{c}{\sigma(1+z_{\text{group}})} \exp \left[\frac{-(c\Delta z)^2}{2\sigma^2(1+z_{\text{group}})^2} \right]. \quad (7)$$

Here we made our main modification by properly taking into account the photometric redshift error, as well as the galaxy velocity dispersion within dark matter halos, with $\sigma = \max(\sigma_{180}, c\sigma_{\text{photo}})$ where σ_{photo} is the typical photometric redshift error listed in Eq. 1. Note that in our galaxy samples, if a galaxy has a spectroscopic redshift,

we assigned it with a $\sigma_{\text{photo}} = 0.0001$ value. For this galaxy, the $\sigma = \sigma_{180}$ value will automatically be used, while for the majority galaxies with only photometric redshifts, $\sigma = c\sigma_{\text{photo}}$.

With the $P_M(\mathbf{R}, \Delta z)$ defined above, we use the following procedure to decide whether a galaxy should be assigned to a particular group. For each galaxy, we loop over all groups to compute the distance $(\mathbf{R}, \Delta z)$ to group center, where \mathbf{R} is the projected distance at the redshift of the cluster. If $P_M(\mathbf{R}, \Delta z) \geq B\sigma_{180}/\sigma$, the galaxy will be assigned to the group. As pointed out in Y05, the background value B in perspective is used as a threshold for the redshift space density contrast of groups. Ideally, for a spectroscopic redshift survey, B should correspond roughly to the redshift space density contrast at the edge of a halo, i.e.,

$$B \approx \frac{\rho_{\text{red}}(r_{180})}{\bar{\rho}} \approx \frac{\rho(r_{180})}{\bar{\rho}} \frac{(4\pi/3)r_{180}^3}{\pi r_{180}^2 \sigma_{180}/H_0}. \quad (8)$$

Using that $\rho(r_{180})/\bar{\rho} \sim 30$ and $\sigma_{180}/H_0 r_{180} \sim 4$, we obtain $B \sim 10$, which is quite independent of halo mass. In this extended group finder, the related background value differs from the original B by a factor of σ_{180}/σ to $B\sigma_{180}/\sigma$, which accounts for the decrease of density contrast caused by the photometric redshift errors.

If a galaxy can be assigned to more than one group according to this criteria, it will be only assigned to the one for with the largest $P_M(\mathbf{R}, \Delta z)$ value. If all members in one group can be assigned to the other group, the two groups will be merged into a single group.

Step 5: Iterate. Using the new memberships obtained in Step 4, we re-compute the group centers and the group luminosity L_G using Eq. 5 and go back to Step 3. This iterative process goes on until there is no further change in the group memberships. Once we finish all the group membership assignment, we go back to Step 1 for another iteration. This iteration cycle stops as long as the mass-to-light ratios have converged, which typically takes only 3 to 4 iterations.

In general, lowering the B value will increase both the completeness and contamination of group members. We note that in Y05 and Y07, the background value (in step 4) is set to $B = 10$ to balance the completeness and contamination of group members. In this work since we aim to extend our algorithm to process photometric galaxy samples, where contamination is inevitable anyway, we focus more on improving the completeness of group/cluster members. For this purpose, in addition to our fiducial $B = 10$ value, we will test the performance of our group finder by adopting a lower B value, e.g., $B = 5$. According to Eq. 8, this lower B value roughly corresponds to consider galaxies that are within $1.5\text{-}\sigma$ photoz error (or velocity dispersion) regions along the line-of-sight.

4. TESTING THE PERFORMANCE OF THE EXTENDED GROUP FINDER

To test the performance of our algorithm we run our extended halo-based group finder over the mock galaxy redshift survey (MGRS) as outlined in section 2.2. This MGRS mimics the depth and photometric redshift quality of the Legacy Surveys DR8.

4.1. Completeness, Contamination, and Purity of the group memberships

To assess the performance of the group finder we proceed as follows: For a group k , we investigate the halo ID for each member galaxy, and sum up the number of members in each halo. We choose the one with the most members as the candidate halo h_k . Since in the photometric data, the brightest central galaxy (BCG) in a halo may move far away from the other members, we do not use the BCG to identify the candidate halo of the group, which is used in Y05. We define N_t as the total number of true members in the MGRS that belong to a halo h_k , N_s is defined as the number of these true members that are selected as members of group k , N_i is defined as the number of interlopers (group members that belong to a different halo) and N_g is defined as the total number of selected group members. These values allow us to define, for each group, the following three quantities:

- The completeness $f_c \equiv N_s/N_t$,
- The contamination $f_i \equiv N_i/N_t$,
- The purity $f_p \equiv N_s/N_g$.

Note that since the contamination is defined with respect to the true number of group members, the contamination f_i can be larger than unity. A contamination $f_i > 1$ implies that the number of interlopers is larger than the number of true members being detected. An ideal group finder yields groups with $f_c = f_p = 1$ and $f_i = 0$.

The results obtained from the MGRS are shown in Fig. 7 with the left panels being for $B = 5$ and the right panels for $B = 10$. Since groups with a single member have zero contamination ($f_i = 0$) by definition, results are only shown for groups with a richness of $N_g \geq 2$. The upper left-hand panel of Fig. 7 shows the cumulative distributions of the completeness f_c for the case of $B = 5$. Different line-styles correspond to groups of different assigned halo mass, M_L , as indicated. There are about 83% groups with group member completeness larger than 80 percent while $\sim 93\%$ of groups have member completeness larger than 60 percent for groups with mass $\gtrsim 10^{12.5} h^{-1} M_\odot$. Among them, groups in the most massive bin shows the highest completeness. The middle left-hand panel of Fig. 7 shows the cumulative distributions of the contamination f_i . On average, around 70% of the groups in mass range $10^{12.5} < \log M_L \leq 10^{14.0} h^{-1} M_\odot$ have $f_i \leq 1$. While in the most massive bin, $10^{14.0} h^{-1} M_\odot < \log M_L$, this number decreases to 43%. Since there are $\sim 30\%$ of the groups with more interlopers than true numbers ($f_i > 1$), special care needs to be taken if one wants to make use of the member galaxies, which we will look into in a subsequent paper. Finally, the lower left-hand panel shows the cumulative distributions of the purity f_p . On average there are about 70% groups with mass $\gtrsim 10^{12.5} h^{-1} M_\odot$ (except those in the most massive bin) having purity $f_p > 0.48$. In the most massive bin, $10^{14.0} h^{-1} M_\odot < \log M_L$, this number is about 41%.

Next, we compute the completeness, contamination, and purity in terms of group membership for our fiducial case of $B = 10$. The corresponding results are shown in the right-hand panels of Fig. 7. Compared to the results shown in the left-hand panels for the case of $B = 5$,

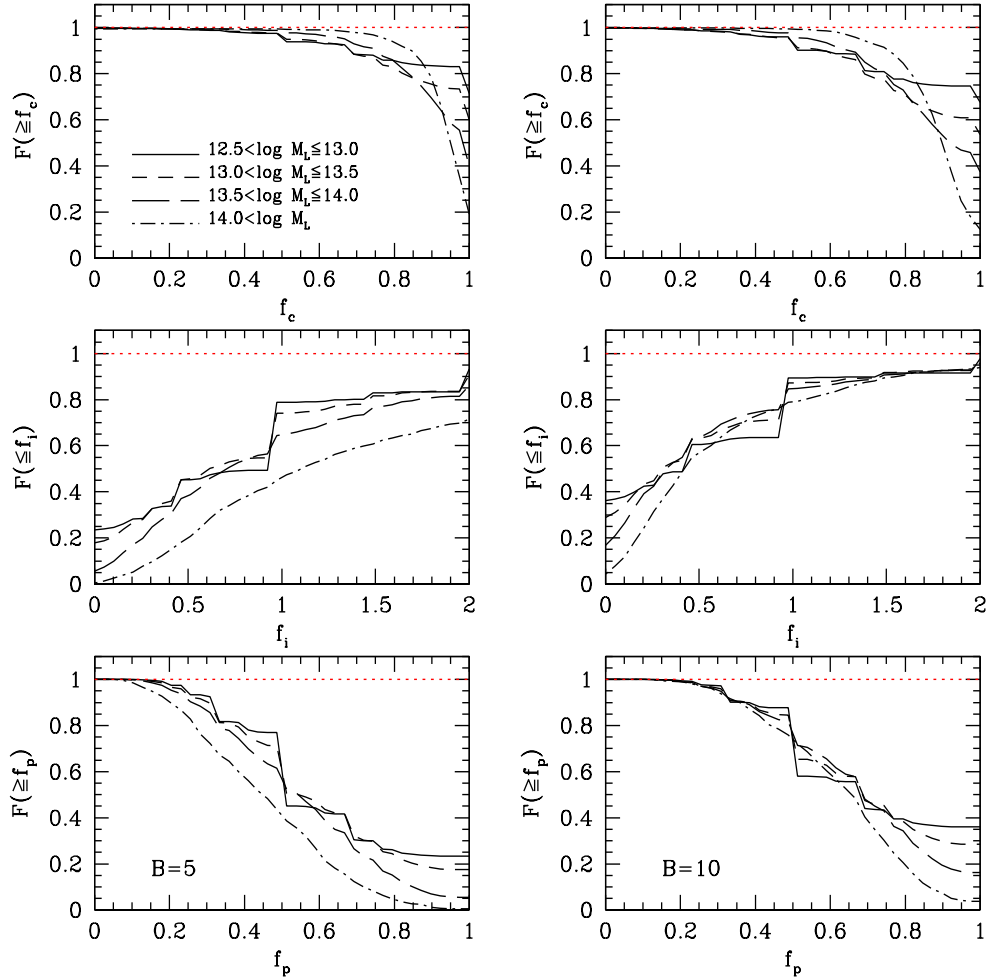


FIG. 7.— The upper, middle and lower panels show the cumulative distributions of completeness, f_c (the fraction of selected true members), contamination, f_i , (the fraction of interlopers), and purity, f_p , (ratio between the selected true members and the group members), respectively. See main text for the detailed definitions of all the above parameters. The left and right panels show the parameters obtained for background values $B = 5$ and $B = 10$, respectively. Different lines show the result for groups with different assigned mass, M_L , as indicated. Results are plotted for groups with at least 2 members, since groups with only 1 member have, by definition, $f_i = 0$.

for groups with mass $10^{12.5} < \log M_L$ the performances differ in the following ways:

- (1) The member completeness is slightly lower. About 72% groups are exhibiting more than 80 percent group member completeness, and $\sim 90\%$ ($\sim 95\%$) groups have member completeness larger than 60 (50) percent.
- (2) The member contamination in each group is smaller than that in the $B = 5$ scenario. Here about 85% of groups have an interloper fraction ≤ 1 .
- (3) The membership purity in each group is also better. About 83% groups having purity $f_p > 0.48$.

Comparing groups in different mass bins, we notice that groups in the highest and lowest mass bins have better completeness and worse purity than groups in the intermediate mass bins. For the case $B=10$, the differences between mass bins are slightly less pronounced.

Given the differences between the $B = 10$ and $B = 5$ cases, if we care more about the purity of the true group members, the case $B = 10$ is preferred.

4.2. Global completeness and purity of the groups

In this subsection, we focus on the global properties of the groups we find from the MGRS. To further evaluate the performance of our extended halo-based group finder, one useful quantity we want to assess is the *global completeness* of groups, f_{halo} , defined as the fraction of halos in the MGRS with more than half of the true members being identified by the group finder as their richest components. The upper left panel of Fig. 8 shows f_{halo} obtained from our MGRS for halos with $N_t \geq 3, 5, 10$ as functions of the true halo mass for the $B = 5$ case. Note that since in our MGRS, the photoz error depends quite strongly on redshift (see Eq. 1), and because of the $z \leq 21$ magnitude cut, groups at higher redshift should have less members and suffer more from the photoz errors. To check the related impact, we separate groups into two redshift bins, $z > 0.5$ and $z \leq 0.5$, where the total number of groups in these two redshift bins are roughly similar. We use red and blue histograms to represents results for groups within these two redshift bins, $z > 0.5$ and $z \leq 0.5$, respectively. We can see that the performance of f_{halo} depends only slightly on the redshift. The group finder successfully selects $\sim 70\%$

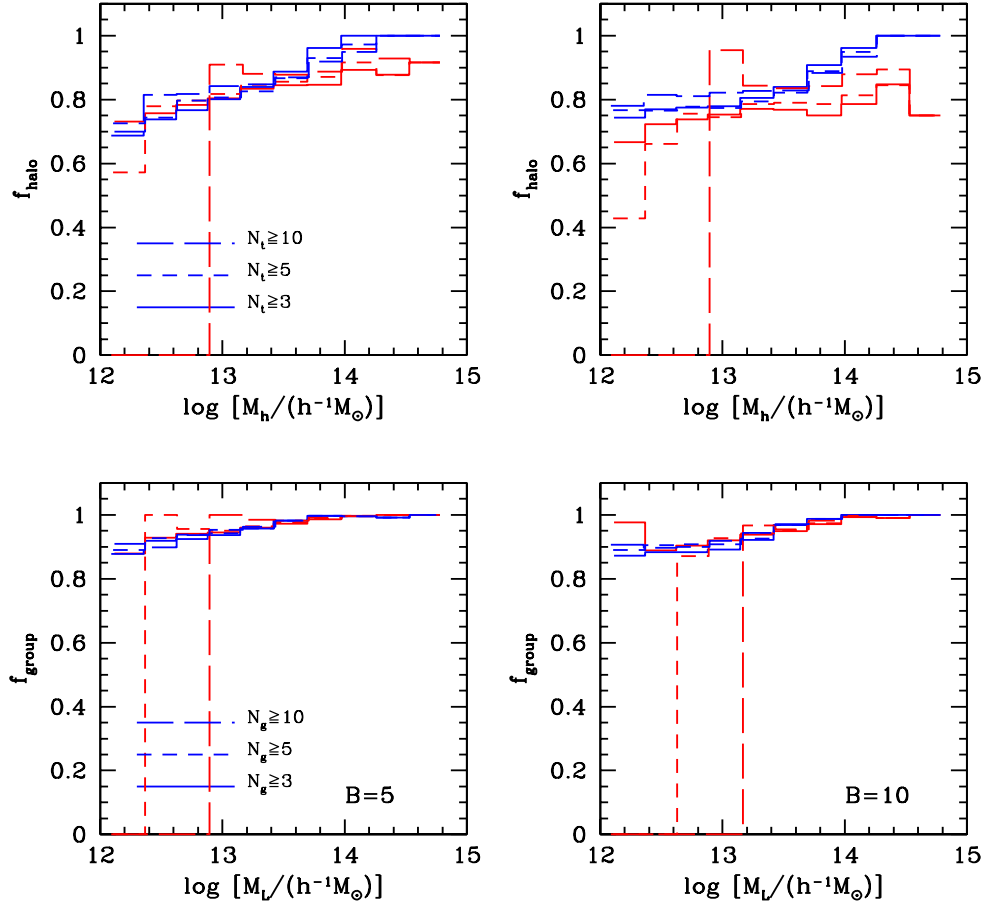


FIG. 8.— Upper panels: The global halo completeness, f_{halo} , defined as the fraction of halos in the MGRS with more than 50% members being identified as the main part of the group, as a function of the true halo mass M_h . Results are shown for halos with at least 3, 5 and 10 true members in the MGRS as indicated, respectively. And we use red and blue histograms to represents results for groups within two redshift bins, $z > 0.5$ and $z \leq 0.5$, respectively. Lower panels: the group purity, f_{group} , defined as the fraction of identified groups which contain more than 50% members of a true halo as a function of the assigned halo mass M_L . Results are shown for groups with at least 3, 5 and 10 identified members, respectively. Here again, we use red and blue histograms to represents results for groups within two redshift bins, $z > 0.5$ and $z \leq 0.5$, respectively. The left and right panels highlight the results obtained for background values of $B = 5$ and $B = 10$, respectively.

($\sim 90\%$) of the true halos with mass $\sim 10^{12} h^{-1}M_\odot$ ($\gtrsim 10^{14} h^{-1}M_\odot$). Note that this does not imply in any case that the $10 \sim 30\%$ of the remaining groups are not selected by our group finder but rather that their group membership completeness is lower than 50%. If we lower the membership completeness criteria, f_{halo} will increase.

The second quantity we investigate is the purity of the groups, f_{group} , defined as the fraction of groups having the richest components that contain more than half of the true members. Here again, we separate groups into two redshift bins, $z > 0.5$ and $z \leq 0.5$, and use red and blue histograms to represents the related results. The lower left panel of Fig. 8 shows f_{group} obtained from our MGRS, for groups with $N_g \geq 3, 5, 10$ as functions of the assigned halo mass for the case $B = 5$. The f_{group} does not show significant differences between the two redshift bins as well. Overall, more than 90% groups with mass $10^{12} h^{-1}M_\odot$ are true groups. The percentage increases as the assigned halo mass and reaches 100% for groups with mass larger than $10^{14.5} h^{-1}M_\odot$. The remaining few groups are those split groups or those whose richest component have less than 50% membership completeness. This value demonstrates that the detected groups regard-

less of their redshifts are in general reliable.

Shown in the right-hand panels of Fig. 8 are the corresponding f_{halo} and f_{group} for the case of $B = 10$. Overall, similar performance is achieved as those in the $B = 5$ case. Except the global completeness in the high redshift bin which is slightly lower, all the other quantities of the detected groups are similar. Note that since f_{halo} corresponds to the fraction of true groups being detected, while f_{group} corresponds to the fraction of the detected groups are true ones. In order to taking into account the impact of incompleteness on the halo mass estimation using the abundance matching method, we correct the abundance of the groups by a factor of $f_{\text{incomp}} = f_{\text{group}}/f_{\text{halo}}$.

4.3. The determination of halo mass and redshift

In this subsection we investigate the reliability of the assigned halo mass and redshift determinations of the groups. First we check the assigned halo mass obtained in the group finding steps 2-3. As pointed out in Y05, our halo mass estimation from the total group luminosity has the advantage that it is equally applicable to groups spanning a wide range in richness. However, a shortcoming of this method is that it requires the halo mass func-

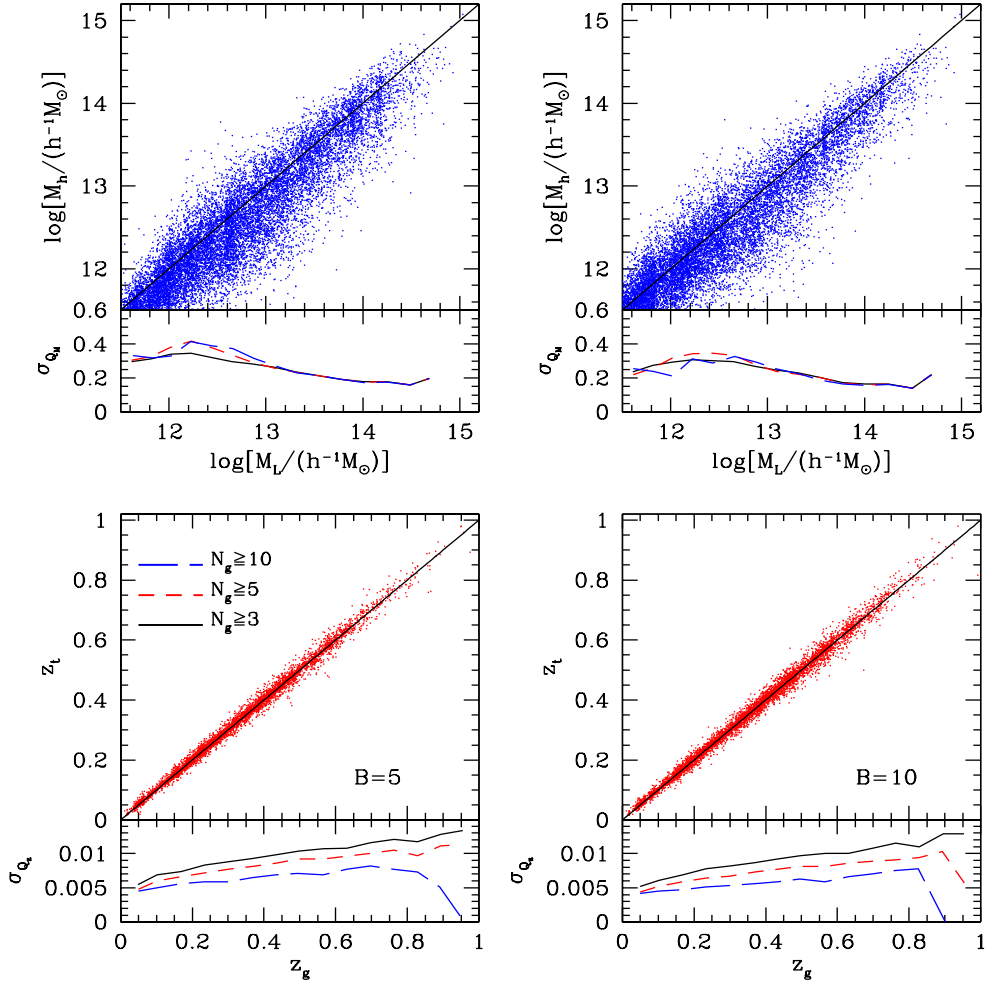


FIG. 9.— Upper panels: Comparisons between the assigned halo mass M_L (based on the total group luminosity L_{tot}) and the true halo mass M_h . The dots are shown for a small subset of groups in the mock group catalog constructed from our MGRS. The small panels plot the scatter from the solid equality line as defined by equation (9). Here, results are shown for groups with different richness cut limits as indicated. Lower panels: comparison between the assigned redshift of the group, z_g , and the true halo redshift z_t . The small sub-panel describes the deviation from the solid equality line. The left and right panels are the results obtained for background values $B = 5$ and $B = 10$, respectively.

tion, which is dependent on cosmology. In general, the assigned halo mass to each group can be regarded as the abundance of its population. Thus, it is extremely easy to convert the retrieved group mass in one cosmology to that in another cosmology, without running another round of group finder.

In order to assess the reliability of the halo mass assigned to individual groups, we use the mock group catalog from the MGRS. The top-left panel of Fig 9 shows the assigned halo mass M_L versus true halo mass M_h in the $B = 5$ case. To quantitatively compare the scatter to the line of equality ($M_L = M_h$), we compute the following quantity for each group

$$Q_M \equiv \frac{1}{\sqrt{2}} [\log(M_L) - \log(M_h)] \quad (9)$$

and measure the standard deviation, σ_{Q_M} , in several bins of $[\log(M_L) + \log(M_h)]/2$. The results shown in the small panel indicate that the scatter is ~ 0.30 dex for groups with $10^{12} h^{-1} M_\odot \lesssim M_L \lesssim 10^{13.0} h^{-1} M_\odot$, decreasing to 0.15 dex at the high mass end. Here we find that the σ_{Q_M} is quite independent of the number of members

in the groups, according to the very similar behaviors shown for groups with different richness cuts.

There are several factors that contribute to this scatter. The first is the intrinsic scatter in the relation between the true halo mass and the true total group luminosity. Here for simplicity, we did not correct for the faint galaxies incompleteness caused by the survey magnitude cut. As shown in the lower right panel of Fig. 5, the mass-to-light ratio has a typical scatter of 0.15 – 0.2 dex. Taking into account the $\sqrt{2}$ factor in Eq. 9, this factor already contribute a lot to the scatter, especially at the high mass end.

The second source of the scatter originates from the incompleteness and contamination introduced by our group finder, which may lead to biased total group luminosities. Nevertheless, as we mentioned before, since we are using the halo abundance matching method to assign halo mass, the systematic difference will not impact our results. Only chaotic difference, e.g., fragmentation or mis-identification will impact the halo mass assignment significantly, which may occur at mass $\lesssim 10^{13.0} h^{-1} M_\odot$ (Campbell et al. 2015).

TABLE 1
NUMBER OF GALAXIES AND GROUPS IN THE DESI IMAGE LEGACY SURVEYS DR8

Region (1)	Galaxies (2)	Sky coverage (3)	Groups $N_g \geq 1$ (4)	$N_g \geq 3$ (5)	$N_g \geq 5$ (6)	$N_g \geq 10$ (7)
NGC	69753872	9673	53335347	2750934	879844	200674
SGC	59598763	8580	45022007	2421063	795323	186841

NOTE. — For each of the NGC or SGC samples, columns (2) and (3) list the number and sky coverage (in unit of square degree) of galaxies. In addition, columns (4)–(7) list the numbers of groups with at least 1, 3, 5, and 10 members.

The last source of scatter in the assigned group masses owes to the fact that groups in the high redshift bin $0.67 < z \leq 1.0$ is incomplete (see the upper-left panel of Fig. 5). Although we have used the V_{\max} method to correct for the incompleteness of groups, since there are scatters among halo masses and BCG luminosities, such corrections are still not enough. The assigned halo mass to our groups will be systematically higher, especially at the low mass end.

Taking into all the above factors into account, we suggest that in our catalog, the groups with mass $\gtrsim 10^{13.0} h^{-1} M_{\odot}$ are more reliable.

Next, we investigate the redshift accuracy of the groups. Shown in the lower left panel of Fig. 9 is the scatter plot of true group redshift z_t v.s. assigned group redshift z_g . Here z_g is defined as the luminosity weight group redshift. To quantify the scatter with respect to the line of equality ($z_t = z_g$), we follow a similar track of halo mass scatter and compute the following quantity for each group

$$Q_z \equiv \frac{1}{\sqrt{2}} \frac{z_t - z_g}{1 + (z_t + z_g)/2} \quad (10)$$

and measure the standard deviation, σ_{Q_z} , in several bins of $[z_t + z_g]/2$. Comparing to the input errors, the results shown in the small panel indicate that the scatter drops with the increase of member galaxies. The typical redshift error in groups with at least 10 members is about 0.008 (taking into account the $\sqrt{2}$ factor in Eq. 10).

Finally, shown in the right hand panels of Fig. 9 are the corresponding mass and redshift determinations for the case of $B = 10$. The general trends are quite similar to the $B = 5$ case, while the mass scatter is somewhat smaller, especially in relatively low mass groups with masses $\lesssim 10^{13.0} h^{-1} M_{\odot}$ at about 0.40 dex (taking into account the $\sqrt{2}$ factor in Eq. 9).

Combining all the above tests, we conclude that the $B = 10$ case performs better than the $B = 5$ case in the group membership purity and halo mass estimation, albeit with somewhat worse group membership completeness. Thus we adopt $B = 10$ value in our group finder for the Legacy Surveys DR8, while $B = 5$ will be used for future comparison studies.

5. BASIC PROPERTIES OF THE GROUP CATALOG

We apply our extended halo-based group finder to the Legacy Surveys DR8 described in Section 2.1. In total, we obtain 53335347 and 45022007 groups in the NGC and SGC, respectively. In the following paragraphs we present some global properties of these group catalogs.

Table 1 lists the results for galaxy samples on the NGC and SGC, respectively for the number of groups with at least 1, 3, 5, and 10 members¹⁷. In total, there are about 5.2 Million groups with at least 3 members, within which about 0.4 million have at least 10 members.

As an illustration, Fig. 10 shows the images of four richest groups in our catalog (two each on the NGC and SGC). In each panel the background image is obtained from the Legacy Surveys DR8 image viewer. The green circle on top of each image illustrates the halo radius, r_{180} , of the group. The location, halo mass and redshift information is marked on the upper-left corner of the image. As an example, the richest group on NGC, located at $ra = 231.1151$, $dec = 29.8872$ at redshift $z = 0.1160$ has 697 member galaxies. For a better illustration, we also mark the locations of all the member galaxies with small red circles. With a careful and zoom in check of these clusters (use the Legacy Surveys DR8 image viewer directly), we can see that there are a few sub-clumps distributed within the halo radius indicating the existence of large sub-structures in massive halos.

Next, we focus on a few statistical quantities for our groups. Shown in the upper-left panel of Fig.11 are the *accumulative* halo mass functions of groups at different redshift bins as indicated. Following the MGRS case, we also show the corresponding theoretical model predictions by SMT2001 using solid lines for a Planck18 cosmology. The data agrees extremely well with the model for the two low redshift bins and are somewhat underestimated at the high redshift bin. Note that since we are using the halo abundance matching method to assign the halo mass, they should agree by construction. The small deviation of the data from the theoretical model predictions for the high redshift bin originates from the *interpolation* of the mass-to-light ratios obtained from different redshift bins.

Shown in the upper-right panel is the richness distribution of groups in the Legacy Surveys DR8. Here we can see that the richest group have about $N_g \sim 700$ members in the low redshift bin, slightly less rich than that in the MGRS. Apart from a few richest clusters, these numbers are roughly consistent with those found in the MGRS after taking into the sky coverage into account. In the high redshift bin, the richest groups have around 30 members which is quite similar to those in the MGRS.

At the lower-left panel we present the *accumulative* total luminosity function of groups in the Legacy Surveys DR8. In the middle and high redshift bins, the groups with $L_{\text{tot}} < 10^{10.0} h^{-2} L_{\odot}$ and $L_{\text{tot}} < 10^{10.6} h^{-2} L_{\odot}$ are

¹⁷ Note that since we might update our group catalogs once additional spectroscopic redshifts are available, the values listed in Tables 1 and 2 are subject to small changes.

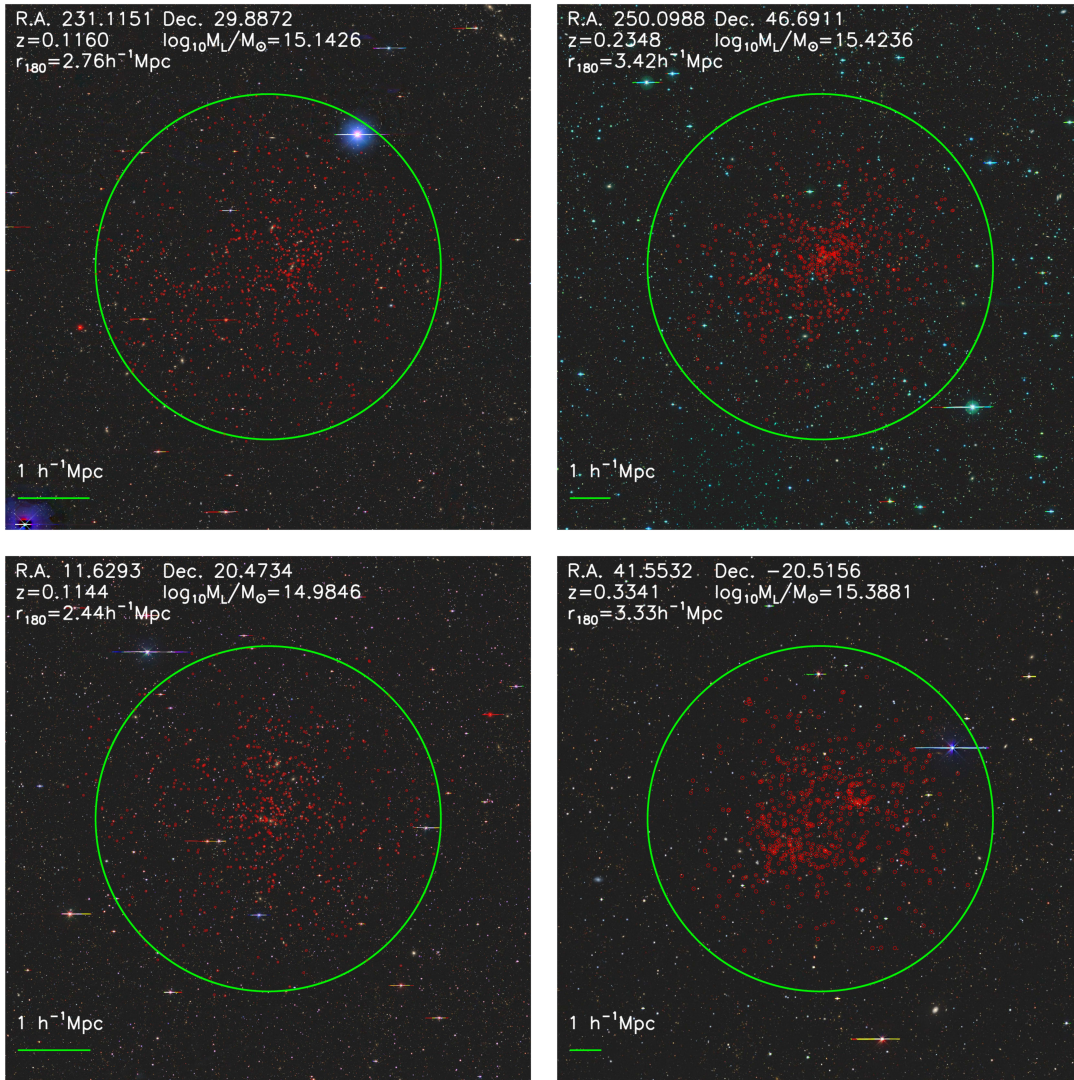


FIG. 10.— Image illustrations of four of the richest groups in our Legacy Surveys DR8 group catalogs. The upper and lower two panels are for two groups in the NGC and SGC, respectively. In each panel the background image is obtained from the Legacy Surveys DR8 image viewer. The green circle illustrates the halo radius, r_{180} , of the group. The small red circles mark the locations of the member galaxies. The location, halo mass and redshift information is marked on the upper-left corner of the image.

missing, which leads to a flattening feature at these luminosities.

Shown at the lower-right panel are the mass-to-light ratio of groups in the Legacy Surveys DR8. The mass-to-light ratios in the two lower redshift bins in groups with mass $\gtrsim 10^{13.5} h^{-1} M_{\odot}$ are in good agreement with each other. While the one at the high redshift bin is higher by roughly 0.1 dex. This is also the main reason that the halo mass function shown in the upper-left panel is underestimated. In groups with mass $\sim 10^{12.0} h^{-1} M_{\odot}$, the mass-to-light ratios show upturns at the lower mass end, which is in general consistent with those CLF model predictions (e.g. Yang et al. 2003).

Finally, for any interested readers in our group catalogs, we have made them publicly available via the following link¹⁸. The data structure and first lines in our catalog are described in Table 2. Since our mass assign-

ments require the use of the halo mass function, which is cosmology dependent, it is very easy to obtain the halo mass for other cosmologies by using the following relation:

$$\int_{M_h}^{\infty} n(M'_h) dM'_h = \int_{\widetilde{M}_h}^{\infty} \widetilde{n}(M'_h) dM'_h, \quad (11)$$

where M_h and $n(M_h)$ are the mass and halo mass function in the Planck18 cosmology, and \widetilde{M}_h and $\widetilde{n}(M_h)$ are the corresponding values in the other cosmology. In addition to the main group catalogs, since we have spectroscopic redshifts for a fraction of galaxies, we will provide a sub-catalog which contains the spectroscopic redshifts for the brightest member galaxies.

6. SUMMARY

In this paper, we extended the halo-based group finder developed in Y05 and Y07, so that it can be applied to

¹⁸ https://gax.sjtu.edu.cn/data/data1/DESI_DR8/groups.tar.gz

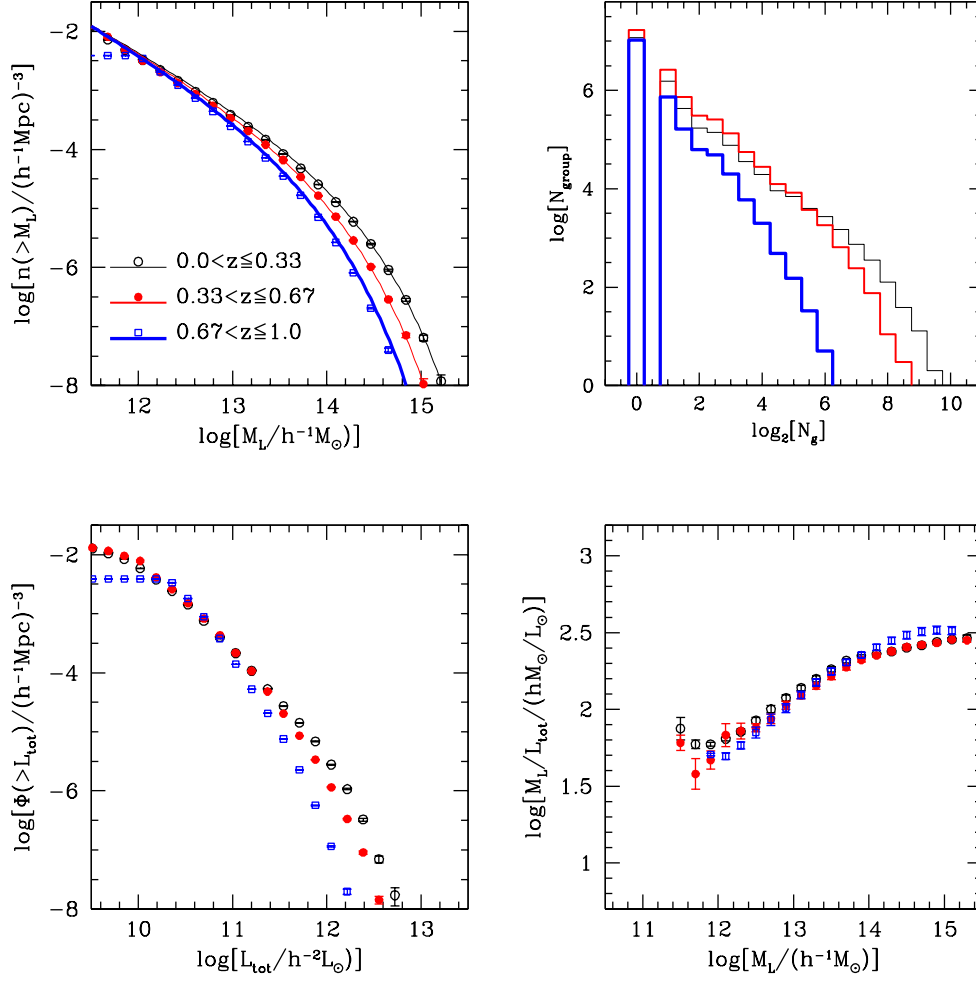


FIG. 11.— Similar to Fig. 5 but here the results are obtained from the Legacy Surveys DR8. The solid lines shown in the upper-left panel are obtained assuming a Planck18 cosmology.

TABLE 2
THE DATA STRUCTURE OF THE LEGACY SURVEYS DR8 GROUP CATALOGS

Group ID (1)	Richness (2)	Ra (3)	dec (4)	redshift (5)	Group mass (6)	Group luminosity (7)
1	697	231.1151	29.8872	0.1160	15.1426	500.3260
2	630	250.0988	46.6911	0.2348	15.4236	818.2732
3	586	229.1876	-0.8609	0.1216	15.1088	456.9565
4	572	213.6720	-0.3643	0.1406	15.1395	496.9307
5	554	127.6793	65.8586	0.1896	15.2778	652.1247
6	486	203.8439	41.0002	0.2386	15.2548	631.4667
7	486	249.0117	66.2045	0.1770	15.1457	503.9358
8	477	260.6339	32.1059	0.2335	15.2154	589.6631
...						
1	551	11.6293	20.4734	0.1144	14.9846	388.9367
2	547	41.5532	-20.5156	0.3341	15.3881	868.7377
3	541	22.9696	-13.5828	0.2186	15.4007	792.0868
4	531	1.5695	-34.7034	0.1214	14.9941	396.0752
5	490	330.3961	-59.9523	0.1066	14.9312	332.6521
6	482	328.4296	-57.7399	0.0791	14.8162	238.3979
7	467	346.3691	-44.2641	0.1373	14.9693	375.2200
8	450	5.5730	23.2938	0.1388	14.9939	395.8793
...						

NOTE. — Column (1): group ID. Column (2): the richness of the group. Columns (3)-(5): the luminosity weighted ra, dec and redshift of the group. Column (6): logarithm of the assigned halo mass $\log M_L$. Column (7): the total group luminosity in unit of $10^{10} h^{-2} L_\odot$. Upper and lower parts are for groups in the NGC and SGC, respectively.

galaxy samples with spectroscopic or photometric redshifts simultaneously. The changes and/or improvements in our group finder are the following:

- We start with our group finder by assuming that all galaxies are tentative groups. We use abundance matching between the total group luminosity and the halo mass to obtain the mass-to-light ratios in an iterative way.
- In order to minimize the impact of the survey magnitude limit to our halo mass estimation, we separate galaxy samples into different redshift bins and obtain their mass-to-light ratios separately. Interpolations in both redshift and group luminosity help obtain the halo mass for each group.
- In the evaluation of the redshift distribution probability function, we also take into account the photometric redshift errors in addition to the galaxy velocity dispersion in halos. This is indeed the most important extension in this version group finder, so that we can treat galaxies with spectroscopic and photometric redshifts equally.
- Apart from the fiducial background value ($B = 10$), we also tested the case with a lower background value ($B = 5$) to enhance the group membership completeness for the photometric redshift samples, which can be used for future comparisons.

Our tests based on a 200 square degree mock galaxy redshift survey (MGRS) with a typical photometric redshift error of $(0.01 + 0.015z) * (1 + z)$ show that for groups with mass $\gtrsim 10^{12.5} h^{-1} M_{\odot}$, $\sim 90\%$ of them have a membership completeness of $> 60\%$. We note that 85% of the groups with mass $\gtrsim 10^{12.5} h^{-1} M_{\odot}$ have an interloper (group members that belong to a different halo) fraction < 1 . In terms of group global properties the group finder can successfully detect more than half members in about 70% and 80% groups with mass $\sim 10^{12.0} h^{-1} M_{\odot}$ and

$\gtrsim 10^{14.0} h^{-1} M_{\odot}$, respectively. For the detected groups with masses $\gtrsim 10^{12.0} h^{-1} M_{\odot}$, the purity (f_{group}) is larger than 90%. The halo mass assigned to each group has an uncertainty of about 0.2 dex at the high mass end $\gtrsim 10^{13.5} h^{-1} M_{\odot}$ and increase to 0.40 dex at the low mass end. The redshift accuracy of the groups with at least 10 members is at ~ 0.008 .

We applied our extended halo-based group finder to the DESI Legacy Imaging Surveys DR8. We obtain separate group catalogs on the north galactic cap (NGC) and south galactic cap (SGC) samples. In the group catalogs, each group is assigned a halo mass, average ra, dec and redshift, etc. Based on these group catalogs, we investigate their basic properties, such as the distributions of richness, halo mass, and luminosity. In addition, we have presented the average ratios between halo mass and group luminosity. A detailed analysis of the group properties and their implications related to halo occupation statistics, galaxy formation and evolution, and cosmology will be presented in a series of forthcoming papers.

ACKNOWLEDGMENTS

We thank the anonymous referee for helpful comments that greatly improved the presentation of this paper. This work is supported by the national science foundation of China (Nos. 11833005, 11890691, 11890692, 11621303, 11890693, 11421303), 111 project No. B20019 and Shanghai Natural Science Foundation, grant No. 15ZR1446700, 19ZR1466800. This work is also supported by the U.D Department of Energy, Office of Science, Office of High Energy Physics under Award Number DE-SC0019301.

This work made use of the Gravity Supercomputer at the Department of Astronomy, Shanghai Jiao Tong University.

The Photometric Redshifts for the Legacy Surveys (PRLS) catalog used in this paper was produced thanks to funding from the U.S. Department of Energy Office of Science, Office of High Energy Physics via grant DE-SC0007914.

REFERENCES

- Avila-Reese, V., Colín, P., González-Samaniego, A., et al. 2011, *ApJ*, 736, 134, doi: 10.1088/0004-637X/736/2/134
- Bahcall, N. A., McKay, T. A., Annis, J., et al. 2003, *ApJS*, 148, 243, doi: 10.1086/377167
- Berlind, A. A., Frieman, J., Weinberg, D. H., et al. 2006, *ApJS*, 167, 1, doi: 10.1086/508170
- Blanton, M. R., & Roweis, S. 2007, *AJ*, 133, 734, doi: 10.1086/510127
- Brown, M. J. I., Zheng, Z., White, M., et al. 2008, *ApJ*, 682, 937, doi: 10.1086/589538
- Cacciato, M., van den Bosch, F. C., More, S., et al. 2009, *MNRAS*, 394, 929, doi: 10.1111/j.1365-2966.2008.14362.x
- Campbell, D., van den Bosch, F. C., Hearin, A., et al. 2015, *Monthly Notices of the Royal Astronomical Society*, 452, 444
- Chen, Y., Mo, H. J., Li, C., et al. 2019, *ApJ*, 872, 180, doi: 10.3847/1538-4357/ab0208
- Coil, A. L., Gerke, B. F., Newman, J. A., et al. 2006, *ApJ*, 638, 668, doi: 10.1086/498885
- Colless, M., Dalton, G., Maddox, S., et al. 2001, *MNRAS*, 328, 1039, doi: 10.1046/j.1365-8711.2001.04902.x
- Collister, A. A., & Lahav, O. 2005, *MNRAS*, 361, 415, doi: 10.1111/j.1365-2966.2005.09172.x
- Crook, A. C., Huchra, J. P., Martimbeau, N., et al. 2007, *ApJ*, 655, 790, doi: 10.1086/510201
- Darvish, B., Mobasher, B., Martin, D. C., et al. 2017, *The Astrophysical Journal*, 837, 16, doi: 10.3847/1538-4357/837/1/16
- Davis, M., Efstathiou, G., Frenk, C. S., & White, S. D. M. 1985, *ApJ*, 292, 371, doi: 10.1086/163168
- Dey, A., Schlegel, D. J., Lang, D., et al. 2019, *AJ*, 157, 168, doi: 10.3847/1538-3881/ab089d
- Díaz-Giménez, E., & Zandivarez, A. 2015, *A&A*, 578, A61, doi: 10.1051/0004-6361/201425267
- Duarte, M., & Mamon, G. A. 2015, *Monthly Notices of the Royal Astronomical Society*, 453, 3849
- Einasto, J., Einasto, M., Tago, E., et al. 2007, *A&A*, 462, 811, doi: 10.1051/0004-6361:20065296
- Eke, V. R., Baugh, C. M., Cole, S., et al. 2004, *MNRAS*, 348, 866, doi: 10.1111/j.1365-2966.2004.07408.x
- Geller, M. J., & Huchra, J. P. 1983, *ApJS*, 52, 61, doi: 10.1086/190859
- Gerke, B. F., Newman, J. A., Davis, M., et al. 2005, *ApJ*, 625, 6, doi: 10.1086/429579
- Goto, T. 2005, *MNRAS*, 359, 1415, doi: 10.1111/j.1365-2966.2005.08982.x
- Goto, T., Sekiguchi, M., Nichol, R. C., et al. 2002, *AJ*, 123, 1807, doi: 10.1086/339303
- Han, J., Eke, V. R., Frenk, C. S., et al. 2015, *Monthly Notices of the Royal Astronomical Society*, 446, 1356, doi: 10.1093/mnras/stu2178
- Hao, J., McKay, T. A., Koester, B. P., et al. 2010, *ApJS*, 191, 254, doi: 10.1088/0067-0049/191/2/254
- Hearin, A. P., & Watson, D. F. 2013, *MNRAS*, 435, 1313, doi: 10.1093/mnras/stt1374

- Huchra, J. P., Macri, L. M., Masters, K. L., et al. 2012, *ApJS*, 199, 26, doi: 10.1088/0067-0049/199/2/26
- Jing, Y. P., Mo, H. J., & Börner, G. 1998, *ApJ*, 494, 1, doi: 10.1086/305209
- Jones, D. H., Read, M. A., Saunders, W., et al. 2009, *MNRAS*, 399, 683, doi: 10.1111/j.1365-2966.2009.15338.x
- Katsianis, A., Xu, H., Yang, X., et al. 2020, arXiv e-prints, arXiv:2010.08173. <https://arxiv.org/abs/2010.08173>
- Kawinwanichakij, L., Quadri, R. F., Papovich, C., et al. 2016, *The Astrophysical Journal*, 817, 9, doi: 10.3847/0004-637X/817/1/9
- Kim, R. S. J., Kepner, J. V., Postman, M., et al. 2002, *AJ*, 123, 20, doi: 10.1086/324727
- Knobel, C., Lilly, S. J., Woo, J., & Kovač, K. 2015, *The Astrophysical Journal*, 800, 24, doi: 10.1088/0004-637X/800/1/24
- Knobel, C., Lilly, S. J., Iovino, A., et al. 2012, *The Astrophysical Journal*, 753, 121
- Koester, B. P., McKay, T. A., Annis, J., et al. 2007, *ApJ*, 660, 239, doi: 10.1086/509599
- Lacey, C., & Cole, S. 1993, *MNRAS*, 262, 627, doi: 10.1093/mnras/262.3.627
- Laigle, C., McCracken, H. J., Ilbert, O., et al. 2016, *The Astrophysical Journal Supplement Series*, 224, 24, doi: 10.3847/0067-0049/224/2/24
- Lan, T.-W., Ménard, B., & Mo, H. 2016, *Monthly Notices of the Royal Astronomical Society*, 459, 3998
- Lang, D., Hogg, D. W., & Mykytyn, D. 2016, *The Tractor: Probabilistic astronomical source detection and measurement*. <http://ascl.net/1604.008>
- Leauthaud, A., Tinker, J., Bundy, K., et al. 2012, *ApJ*, 744, 159, doi: 10.1088/0004-637X/744/2/159
- Lee, B. C., Allam, S. S., Tucker, D. L., et al. 2004, *AJ*, 127, 1811, doi: 10.1086/382236
- Li, R., Mo, H. J., Fan, Z., Bosch, F. C. v. d., & Yang, X. 2011, *Monthly Notices of the Royal Astronomical Society*, 413, 3039, doi: 10.1111/j.1365-2966.2011.18378.x
- Lim, S., Mo, H., Wang, H., & Yang, X. 2020, *The Astrophysical Journal*, 889, 48
- Lim, S. H., Mo, H. J., Li, R., et al. 2018, *The Astrophysical Journal*, 854, 181, doi: 10.3847/1538-4357/aaaa21
- Lim, S. H., Mo, H. J., Lu, Y., Wang, H., & Yang, X. 2017, *MNRAS*, 470, 2982, doi: 10.1093/mnras/stx1462
- Lu, Y., Yang, X., & Shen, S. 2015, *ApJ*, 804, 55, doi: 10.1088/0004-637X/804/1/55
- Lu, Y., Yang, X., Shi, F., et al. 2016, *ApJ*, 832, 39, doi: 10.3847/0004-637X/832/1/39
- Luo, W., Yang, X., Lu, T., et al. 2018, *The Astrophysical Journal*, 862, 4
- Macciò, A. V., Dutton, A. A., van den Bosch, F. C., et al. 2007, *MNRAS*, 378, 55, doi: 10.1111/j.1365-2966.2007.11720.x
- Mandelbaum, R., Seljak, U., Cool, R. J., et al. 2006, *Monthly Notices of the Royal Astronomical Society*, 372, 758, doi: 10.1111/j.1365-2966.2006.10906.x
- Meng, J., Li, C., Mo, H., Chen, Y., & Wang, K. 2020, arXiv e-prints, arXiv:2008.13733. <https://arxiv.org/abs/2008.13733>
- Merchán, M., & Zandivarez, A. 2002, *MNRAS*, 335, 216, doi: 10.1046/j.1365-8711.2002.05623.x
- Merchán, M. E., & Zandivarez, A. 2005, *ApJ*, 630, 759, doi: 10.1086/427989
- Miller, C. J., Nichol, R. C., Reichart, D., et al. 2005, *AJ*, 130, 968, doi: 10.1086/431357
- Mo, H., van den Bosch, F. C., & White, S. 2010, *Galaxy Formation and Evolution*
- More, S., van den Bosch, F. C., Cacciato, M., et al. 2009, *MNRAS*, 392, 801, doi: 10.1111/j.1365-2966.2008.14095.x
- Navarro, J. F., Frenk, C. S., & White, S. D. M. 1997, *ApJ*, 490, 493, doi: 10.1086/304888
- Neistein, E., Weinmann, S. M., Li, C., & Boylan-Kolchin, M. 2011, *MNRAS*, 414, 1405, doi: 10.1111/j.1365-2966.2011.18473.x
- Oguri, M., Lin, Y.-T., Lin, S.-C., et al. 2018, *PASJ*, 70, S20, doi: 10.1093/pasj/psx042
- Peacock, J. A., & Smith, R. E. 2000, *MNRAS*, 318, 1144, doi: 10.1046/j.1365-8711.2000.03779.x
- Planck Collaboration, Aghanim, N., Akrami, Y., et al. 2020, *A&A*, 641, A6, doi: 10.1051/0004-6361/201833910
- Raichoor, A., Eisenstein, D. J., Karim, T., et al. 2020, *Research Notes of the American Astronomical Society*, 4, 180, doi: 10.3847/2515-5172/abc078
- Robotham, A., Wallace, C., Philipps, S., & De Propris, R. 2006, *ApJ*, 652, 1077, doi: 10.1086/508130
- Rodriguez, F., & Merchán, M. 2020, *A&A*, 636, A61, doi: 10.1051/0004-6361/201937423
- Rodriguez, F., Merchán, M., & Sgró, M. A. 2015, *Astronomy & Astrophysics*, 580, A86, doi: 10.1051/0004-6361/201525798
- Ruiz-Macias, O., Zarrouk, P., Cole, S., et al. 2020, *Research Notes of the American Astronomical Society*, 4, 187, doi: 10.3847/2515-5172/abc25a
- Rykoff, E. S., Rozo, E., Busha, M. T., et al. 2014, *ApJ*, 785, 104, doi: 10.1088/0004-637X/785/2/104
- Sheth, R. K., Mo, H. J., & Tormen, G. 2001, *MNRAS*, 323, 1, doi: 10.1046/j.1365-8711.2001.04006.x
- Springel, V. 2005, *MNRAS*, 364, 1105, doi: 10.1111/j.1365-2966.2005.09655.x
- Szabo, T., Pierpaoli, E., Dong, F., Pipino, A., & Gunn, J. 2011, *ApJ*, 736, 21, doi: 10.1088/0004-637X/736/1/21
- Tago, E., Einasto, J., Saar, E., et al. 2006, *Astronomische Nachrichten*, 327, 365, doi: 10.1002/asna.200510536
- Tinker, J. L. 2020, arXiv e-prints, arXiv:2010.02946. <https://arxiv.org/abs/2010.02946>
- Tinker, J. L., Weinberg, D. H., Zheng, Z., & Zehavi, I. 2005, *ApJ*, 631, 41, doi: 10.1086/432084
- Tucker, D. L., Oemler, Augustus, J., Hashimoto, Y., et al. 2000, *ApJS*, 130, 237, doi: 10.1086/317348
- van den Bosch, F. C., Norberg, P., Mo, H. J., & Yang, X. 2004, *MNRAS*, 352, 1302, doi: 10.1111/j.1365-2966.2004.08021.x
- van den Bosch, F. C., Weinmann, S. M., Yang, X., et al. 2005, *MNRAS*, 361, 1203, doi: 10.1111/j.1365-2966.2005.09260.x
- van den Bosch, F. C., Yang, X., & Mo, H. J. 2003, *MNRAS*, 340, 771, doi: 10.1046/j.1365-8711.2003.06335.x
- van den Bosch, F. C., Yang, X., Mo, H. J., et al. 2007, *MNRAS*, 376, 841, doi: 10.1111/j.1365-2966.2007.11493.x
- Vikram, V., Lidz, A., & Jain, B. 2017, *Monthly Notices of the Royal Astronomical Society*, stw3311, doi: 10.1093/mnras/stw3311
- Viola, M., Cacciato, M., Brouwer, M., et al. 2015, *Monthly Notices of the Royal Astronomical Society*, 452, 3529, doi: 10.1093/mnras/stv1447
- Wang, H., Mo, H. J., Yang, X., Jing, Y. P., & Lin, W. P. 2014, *ApJ*, 794, 94, doi: 10.1088/0004-637X/794/1/94
- Wang, H., Mo, H. J., Yang, X., et al. 2016, *The Astrophysical Journal*, 831, 164, doi: 10.3847/0004-637X/831/2/164
- Wang, H., Mo, H., Chen, S., et al. 2018, *The Astrophysical Journal*, 852, 31
- Wang, H., Mo, H. J., Chen, S., et al. 2018, *ApJ*, 852, 31, doi: 10.3847/1538-4357/aa9e01
- Wang, K., Mo, H. J., Li, C., Meng, J., & Chen, Y. 2020. <https://arxiv.org/abs/2006.05426>
- Wei, C., Li, G., Kang, X., et al. 2018, *ApJ*, 853, 25, doi: 10.3847/1538-4357/aaa40d
- Weinmann, S. M., van den Bosch, F. C., Yang, X., & Mo, H. J. 2006, *MNRAS*, 366, 2, doi: 10.1111/j.1365-2966.2005.09865.x
- Wen, Z. L., Han, J. L., & Liu, F. S. 2012, *ApJS*, 199, 34, doi: 10.1088/0067-0049/199/2/34
- Willmer, C. N. A. 2018, *ApJS*, 236, 47, doi: 10.3847/1538-4365/aabfd4
- Yang, X., Mo, H. J., Jing, Y. P., & van den Bosch, F. C. 2005a, *MNRAS*, 358, 217, doi: 10.1111/j.1365-2966.2005.08801.x
- Yang, X., Mo, H. J., & van den Bosch, F. C. 2003, *MNRAS*, 339, 1057, doi: 10.1046/j.1365-8711.2003.06254.x
- 2006, *ApJ*, 638, L55, doi: 10.1086/501069
- Yang, X., Mo, H. J., & van den Bosch, F. C. 2008, *The Astrophysical Journal*, 676, 248, doi: 10.1086/528954
- 2009, *The Astrophysical Journal*, 695, 900, doi: 10.1088/0004-637X/695/2/900
- Yang, X., Mo, H. J., van den Bosch, F. C., & Jing, Y. P. 2005b, *MNRAS*, 356, 1293, doi: 10.1111/j.1365-2966.2005.08560.x
- 2005c, *MNRAS*, 357, 608, doi: 10.1111/j.1365-2966.2005.08667.x
- Yang, X., Mo, H. J., van den Bosch, F. C., et al. 2007, *ApJ*, 671, 153, doi: 10.1086/522027
- 2005d, *MNRAS*, 362, 711, doi: 10.1111/j.1365-2966.2005.09351.x
- Yang, X., Mo, H. J., van den Bosch, F. C., Zhang, Y., & Han, J. 2012, *ApJ*, 752, 41, doi: 10.1088/0004-637X/752/1/41
- Yang, X., Zhang, Y., Wang, H., et al. 2018, *ApJ*, 860, 30, doi: 10.3847/1538-4357/aac2ce
- Yèche, C., Palanque-Delabrouille, N., Claveau, C.-A., et al. 2020, *Research Notes of the American Astronomical Society*, 4, 179, doi: 10.3847/2515-5172/abc01a
- Zandivarez, A., Martínez, H. J., & Merchán, M. E. 2006, *ApJ*, 650, 137, doi: 10.1086/503894
- Zheng, Z., Berlind, A. A., Weinberg, D. H., et al. 2005, *ApJ*, 633, 791, doi: 10.1086/466510
- Zhou, R., Newman, J. A., Mao, Y.-Y., et al. 2020a, arXiv e-prints, arXiv:2001.06018. <https://arxiv.org/abs/2001.06018>
- Zhou, R., Newman, J. A., Dawson, K. S., et al. 2020b, *Research Notes of the American Astronomical Society*, 4, 181, doi: 10.3847/2515-5172/abc0f4
- Zou, H., Gao, J., Zhou, X., & Kong, X. 2019, *ApJS*, 242, 8, doi: 10.3847/1538-4365/ab1847